Lack of GLYCOLATE OXIDASE1, but Not GLYCOLATE OXIDASE2, Attenuates the Photorespiratory Phenotype of CATALASE2-Deficient Arabidopsis[1][OPEN]

Pavel Kerchev[2], Cezary Waszczak[2], Aleksandra Lewandowska, Patrick Willems, Alexey Shapiguzov, Zhen Li, Saleh Alseekh, Per Mühlenbock, Frank A. Hoeberichts, Jingjing Huang, Katrien Van Der Kelen, Jaakko Kangasjärvi, Alisdair R. Fernie, Riet De Smet, Yves Van de Peer, Joris Messens, and Frank Van Breusegem*

Department of Plant Systems Biology, VIB, 9052 Ghent, Belgium (P.K., C.W., A.L., P.W., Z.L., P.M., F.A.H., K.V.D.K., R.D.S. Y.V.d.P., F.V.B.); Department of Plant Biotechnology and Bioinformatics, Ghent University, 9052 Ghent, Belgium (P.K., C.W., A.L., P.W., Z.L., P.M., F.A.H., K.V.D.K., R.D.S., Y.V.d.P., F.V.B.); Structural Biology Research Center, VIB, 1050 Brussels, Belgium (C.W., A.L., J.H., J.M.); Structural Biology Brussels Laboratory, Vrije Universiteit Brussel, 1050 Brussels, Belgium (C.W., A.L., J.H., J.M.); Brussels Center for Redox Biology, 1050 Brussels, Belgium (C.W., A.L., J.H., J.M.); Division of Plant Biology, Viikki Plant Science Centre, Department of Biosciences, University of Helsinki, Helsinki FI-00014, Finland (C.W., A.S., J.K.); Institute of Plant Physiology, Russian Academy of Sciences, 127276 Moscow, Russia (A.S.); Max-Planck-Institute for Molecular Plant Physiology, 14476 Potsdam-Golm, Germany (S.A., A.R.F.); Distinguished Scientist Fellowship Program, College of Science, King Saud University, Riyadh, Saudi Arabia (J.K.); and Genomics Research Institute, University of Pretoria, Pretoria, South Africa (Y.V.d.P.)

ORCID IDs: 0000-0003-2737-0493 (P.K.); 0000-0003-4667-2294 (P.W.); 0000-0001-8920-9270 (Z.L.); 0000-0003-3097-8387 (P.M.); 0000-0002-8959-1809 (J.K.); 0000-0002-3147-0860 (F.V.B.).

The genes coding for the core metabolic enzymes of the photorespiratory pathway that allows plants with C3-type photosynthesis to survive in an oxygen-rich atmosphere, have been largely discovered in genetic screens aimed to isolate mutants that are unviable under ambient air. As an exception, glycolate oxidase (GOX) mutants with a photorespiratory phenotype have not been described yet in C3 species. Using Arabidopsis (*Arabidopsis thaliana*) mutants lacking the peroxisomal *CATALASE2* (*cat2-2*) that display stunted growth and cell death lesions under ambient air, we isolated a second-site loss-of-function mutation in *GLYCOLATE OXIDASE1* (*GOX1*) that attenuated the photorespiratory phenotype of *cat2-2*. Interestingly, knocking out the nearly identical *GOX2* in the *cat2-2* background did not affect the photorespiratory phenotype, indicating that GOX1 and GOX2 play distinct metabolic roles. We further investigated their individual functions in single *gox1-1* and *gox2-1* mutants and revealed that their phenotypes can be modulated by environmental conditions that increase the metabolic flux through the photorespiratory pathway. High light negatively affected the photosynthetic performance and growth of both *gox1-1* and *gox2-1* mutants, but the negative consequences of severe photorespiration were more pronounced in the absence of GOX1, which was accompanied with lesser ability to process glycolate. Taken together, our results point toward divergent functions of the two photorespiratory GOX isoforms in Arabidopsis and contribute to a better understanding of the photorespiratory pathway.

The increase in atmospheric CO_2 levels linked to global warming, which entails unpredictable climate conditions, poses an unprecedented pressure on modern agriculture (Lobell and Gourdji, 2012; Wheeler and von Braun, 2013). However, apart from its greenhouse properties, CO_2 and its photosynthetic assimilation into biomass are the primary foundation of life on Earth. Thus, atmospheric CO_2 content has a direct effect on agricultural production, and even a modest CO_2 increase might in theory result in higher crop yields, especially in plants with C3-type photosynthesis (Walker et al., 2016). In contrast to C4 and CAM-type plants, C3 plants do not possess carbon concentrating mechanisms, and the first stable CO_2 assimilation product is 3-phosphoglycerate that is further processed in the Calvin-Benson cycle to fuel sugar synthesis. C4 plants initially incorporate CO_2 into four-carbon acids that are subsequently decarboxylated in the vicinity of the primary CO_2-assimilating enzyme Rubisco. The C4-type photosynthesis evolved independently over 60 times (Sage et al., 2011), reflecting the need to counteract the highly promiscuous nature of Rubisco that apart from carboxylation of ribulose-1,5-bisphosphate also catalyzes its oxygenation to 2-phosphoglycolate (PG). This oxygenation reaction initiates the photorespiratory pathway that recycles PG back to 3-phosphoglycerate with the release of CO_2 in a series of enzymatic steps distributed between chloroplasts, peroxisomes, and mitochondria (Timm et al., 2008; Bauwe et al., 2012). The metabolic flux through the photorespiratory pathway increases substantially under adverse environmental conditions, such as drought and heat, which

ultimately result in a loss of assimilated CO_2 and a consequent yield reduction (Walker et al., 2016).

The photorespiratory pathway supports the second highest metabolic flux in photosynthesizing tissues after the Calvin-Benson cycle. Although the core photorespiratory pathway is now elucidated at the enzymatic level, its functional significance beyond carbon recycling and intimate interplay with primary metabolism remains a matter of debate (Bauwe et al., 2012; Hodges et al., 2016). Moreover, the existence of bypasses for core photorespiratory intermediates that play an important role during stress conditions imposes additional difficulties in elucidating the fine-tuning of the photorespiratory pathway (Timm et al., 2008, 2011). In the photorespiratory pathway, PG is first dephosphorylated by phosphoglycolate phosphatase to glycolate, which is subsequently exported from the chloroplasts via the plastidial glycolate/glycerate translocator 1 (Pick et al., 2013). Glycolate then undergoes oxidation in the peroxisomes catalyzed by the tetrameric FMN-dependent glycolate oxidase (GOX; EC 1.1.3.15), which generates glycoxylate and H_2O_2.

Arabidopsis (*Arabidopsis thaliana*) mutants lacking peroxisomal CATALASE2 (*cat2-2*) display around 10% wild-type catalase activity and have been instrumental in elucidating the impact of elevated photorespiratory H_2O_2 on the induction of defense responses and cell death (Queval et al., 2007; Kaurilind et al., 2015). The increase of H_2O_2 levels in *cat2-2* mutants can be conditionally controlled by modulation of the growth environment. Restriction of the influx of fresh air to in vitro-grown plants, for example, decreases the available CO_2 and ultimately results in enhanced photorespiration (Kerchev et al., 2015). Under such conditions, *cat2-2* mutants display a rapid decline of photosynthetic activity and eventual cell death. In contrast, growing *cat2-2* mutants under high CO_2 atmosphere limits the rate of photorespiration and thus renders them indistinguishable from the wild type. Transfer of high CO_2-grown *cat2-2* mutants to photorespiration-promoting conditions, such as high light and ambient air, activates the photorespiratory pathway and triggers profound transcriptional and metabolic rearrangements and lesion formation (Queval et al., 2007).

The Arabidopsis genome contains five genes annotated as enzymes with GOX activity (Rojas et al., 2012; Hodges et al., 2013). They form the (L)-2-hydroxyacid-oxidases [(L)-2-HAOX] family that contains *GOX1* (*At3g14420*), *GOX2* (*At3g14415*), *GOX3* (*At4g18360*), *HAOX1* (*At3g14130*), and *HAOX2* (*At3g14150*). GOX1 and GOX2 are the major isoforms found in leaf peroxisomes (Reumann et al., 2007; Foyer et al., 2009; Dellero et al., 2016). GOX3, on the other hand, is mainly expressed in roots where it converts glycolate and L-lactate with similar efficiency, making it an important player in lactate metabolism (Engqvist et al., 2015). HAOX1 and HAOX2 act predominantly on medium- and long-chain hydroxy acids, show a negligible activity toward glycolate (Esser et al., 2014), and are mainly expressed in seeds (Hodges et al., 2013).

Despite having only 30% residual GOX activity, single mutants lacking GOX1 or GOX2 show no visible phenotype implying a certain degree of functional redundancy (Rojas et al., 2012; Dellero et al., 2016). Moreover, recombinant GOX1 and GOX2 proteins exhibit similar kinetic parameters (Dellero et al., 2015). *GOX1* and *GOX2* reside in a tandem repeat on chromosome 3. The two homologs are separated by a mere 890 bp, which precludes the generation of double *gox1 gox2* mutants through crossing of the available T-DNA insertion mutants. However, simultaneously knocking down *GOX1* and *GOX2* by artificial microRNA resulted in 5% residual GOX activity and stunted growth in ambient air (Dellero et al., 2016). Thus far, mutants affected in GOX activity have not been isolated in photorespiratory mutant screens in C3 species (Timm and Bauwe, 2013). The only example of a single GOX mutation that results in a photorespiratory phenotype is *Zmgo1* in the C4 plant maize (*Zea mays*; Zelitch et al., 2009). In rice (*Oryza sativa*), an antisense-based strategy was employed to suppress the redundant *GOX* genes and to inhibit the flux through the photorespiratory pathway to levels negatively affecting photosynthesis and growth (Xu et al., 2009).

In a second-site suppressor screen for mutations attenuating the photorespiratory phenotype of Arabidopsis plants lacking peroxisomal catalase (*cat2-2*), we isolated a causative loss-of-function mutation in the *GOX1* gene. Interestingly, the introduction of the *gox2-1* allele into the *cat2-2* background did not prevent the negative effects of photorespiration and the double

[1] This work was supported by grants from Ghent University Multidisciplinary Research Partnership "Sustainable BioEconomy" (project 01MRB510W), the Interuniversity Attraction Poles Program (IUAP P7/29), and the Research Foundation-Flanders (grant no. G0D7914N). C.W. and A.L are indebted to VIB International PhD Program for a predoctoral fellowship, and P.K. is a recipient of Omics@VIB Marie Curie COFUND and FWO Pegasus fellowships. P.M. was a recipient of a Marie Curie Intra-European Fellowships for Career Development (PIEF-GA-2009-235827). R.D.S. is a postdoctoral fellow of The Research Foundation-Flanders (FWO). The work was partially funded by the Deutsche Forschungsgemeinschaft through the Forscher-gruppe FOR 1186 (Promics; A.R.F.) and the Academy of Finland Centre of Excellence Program (2014-19). This work was also supported by IWT (projects Phoenix and Stressnet).

[2] These authors contributed equally to the article.

* Address correspondence to frank.vanbreusegem@psb.vib-ugent.be.

The author responsible for distribution of materials integral to the findings presented in this article in accordance with the policy described in the Instructions for Authors (www.plantphysiol.org) is: Frank Van Breusegem (frank.vanbreusegem@psb.vib-ugent.be).

P.K., C.W., and F.V.B conceived the project, designed and performed the experiments, and wrote the article with contribution of all coauthors; Z.L. performed the evolutionary analysis supervised by R.D.S. and Y.V.d.P.; S.A. performed the metabolite measurements supervised by A.R.F., P.M., F.A.H., K.V.D.K., and F.V.B. conceived the original mutant screen; A.L. and J.H. performed experiments supervised by J.M.; A.S. and C.W. performed the photosynthetic measurements supervised by J.K.; P.W. analyzed the RNA-seq data.

[OPEN] Articles can be viewed without a subscription.

www.plantphysiol.org/cgi/doi/10.1104/pp.16.00359

cat2-2 gox2-1 mutants phenocopied the parental *cat2-2* plants. Using a series of physiological, biochemical, and metabolomic approaches, we investigated the differential photorespiratory response of *cat2-2* mutants in the absence of *GOX1* and *GOX2*. Our results reveal the existence of nonredundant functions for GOX1 and GOX2 and contribute to a better understanding of the enzymes involved in the photorespiratory pathway.

RESULTS

Lack of GOX1, But Not GOX2, Attenuates the Photorespiratory Phenotype of Arabidopsis Plants Deficient in Peroxisomal Catalase

We previously conducted a high-throughput suppressor screen for second-site mutations that alleviate the photorespiratory phenotype of Arabidopsis plants lacking peroxisomal catalase (*cat2-2*; Waszczak et al., 2016). This screening strategy involved restriction of gas exchange to in vitro-grown plants and exposure to continuous light to avoid respiratory CO_2 buildup. Under these conditions, *cat2-2* mutants display a rapid decline of PSII maximum efficiency (F_v'/F_m') and cell death within 7 d from the onset of the treatment (Vanderauwera et al., 2011; Kerchev et al., 2015).

One of the mutants isolated in the screen, referred to here as *238.3*, mitigated the characteristic F_v'/F_m' decline and cell death observed in single *cat2-2* mutants under photorespiration-promoting conditions (Fig. 1, A–C). Using the SHOREmap backcross strategy (Hartwig et al., 2012; see "Materials and Methods"), the causative mutation was mapped to an intron-exon junction in the gene encoding GOX1 (Fig. 1D). Foliar GOX activity in *238.3* was reduced by more than 50% in comparison to single *cat2-2* mutants (Fig. 1E), suggesting that the identified single-nucleotide polymorphism generates a loss-of-function mutation.

To confirm that lack of GOX1 is responsible for the attenuation of the photorespiratory phenotype observed in *238.3*, we introduced the T-DNA insertion allele *gox1-1* (Supplemental Fig. S1) into the *cat2-2* background and exposed the resulting *cat2-2 gox1-1* double mutants (Supplemental Fig. S2) to the same photorespiratory stress as applied in the original high-throughput screen. Under these conditions, *cat2-2 gox1-1* mutants retained higher F_v'/F_m' values and exhibited limited cell death in comparison to single *cat2-2* mutants (Fig. 2, A–C). We further tested whether the protective effect of *gox1-1* can be similarly observed in soil-grown plants exposed to severe photorespiratory conditions. To this end, 3-week-old plants grown under high CO_2 atmosphere (3,000 μL L^{-1}), aimed to limit photorespiration, were exposed to high light (~1,000 μmol m^{-2} s^{-1}) and ambient air. The transfer resulted in cell death lesion formation in *cat2-2* mutants within 24 h, whereas *cat2-2 gox1-1* double mutants were largely unaffected and survived the photorespiratory stress (Fig. 2D).

To test whether the loss of any other glycolate-metabolizing enzyme from the (L)-2-HAOX family, apart from GOX1, might attenuate of the photorespiratory phenotype of *cat2-2*, we generated a series of double (*cat2-2 gox2-1*, *cat2-2 gox3-1*, *cat2-2 haox1-1*, and *cat2-2 haox2-1*) and triple (*cat2-2 gox1-1 gox3-1*) mutants and assessed their phenotype under photorespiratory stress. Surprisingly, knocking out *GOX2*, the other predicted photorespiratory GOX isoform, in the *cat2-2* background did not alleviate the cell death of *cat2-2 gox2-1* double mutants under in vitro and in soil photorespiration-promoting conditions (Fig. 3, A–C). Similarly, introduction of either *haox1-1* or *haox2-1* alleles into the *cat2-2* background had no effect on the photorespiratory phenotype (Fig. 3, A–C). The *cat2-2 gox3-1* double mutants were indistinguishable from the parental *cat2-2* plants under photorespiration-promoting conditions (Fig. 3, A–C), which is in line with the notion that GOX3 is active predominantly in roots. Moreover, the negative effects of photorespiration in *cat2-2 gox1-1 gox3-1* triple mutants were attenuated to the same extent as in *cat2-2 gox1-1* double mutants (Fig. 3, A–C), implying that the combined loss of GOX3 and GOX1 does not have an additive effect.

Our genetic analysis indicated that the lack of GOX3, HAOX1, and HAOX2 does not influence the photorespiratory phenotype of *cat2-2*, which is in line with their substrate preferences and tissue-specific expression (Hodges et al., 2013; Esser et al., 2014; Engqvist et al., 2015). GOX1 and GOX2, on the other hand, metabolize glycolate in vitro with similar kinetic parameters and have been assumed to equally support the photorespiratory pathway. We therefore set out to investigate the differential response of *cat2-2 gox1-1* and *cat2-2 gox2-1* mutants under photorespiratory stress.

Global Transcriptome and Metabolome Rearrangements Accompanying the Increased Survival of *cat2-2 gox1-1* Mutants under Photorespiratory Stress

To gain insight into the early events underlying the attenuation of the photorespiratory phenotype of *cat2-2* in the absence of GOX1, we performed global transcriptome (RNA-seq) and metabolome (gas chromatography-mass spectrometry [GC-MS]) profiling of high-CO_2-grown plants before and after exposure to photorespiratory stress. Only 14 transcripts showed differential regulation ($|\log_2 FC| > 1$, FDR < 0.05) between *cat2-2 gox1-1* and *cat2-2 gox2-1* mutants relative to *cat2-2* under control high CO_2 conditions, implying that all genotypes are comparable (Supplemental Fig. S3). The transfer to photorespiratory stress (high light and ambient air) triggered a profound transcriptional response with 5,876 differentially regulated genes ($|\log_2 FC| > 1$, FDR < 0.01) after 3 h in *cat2-2* mutants (Fig. 4A; Supplemental Data Set 1). The majority of the transcripts (3,808) were induced, while 2,068 were repressed. A significant transcriptional overlap (2,798 common up- and 1,213 down-regulated transcripts) was observed between the tested

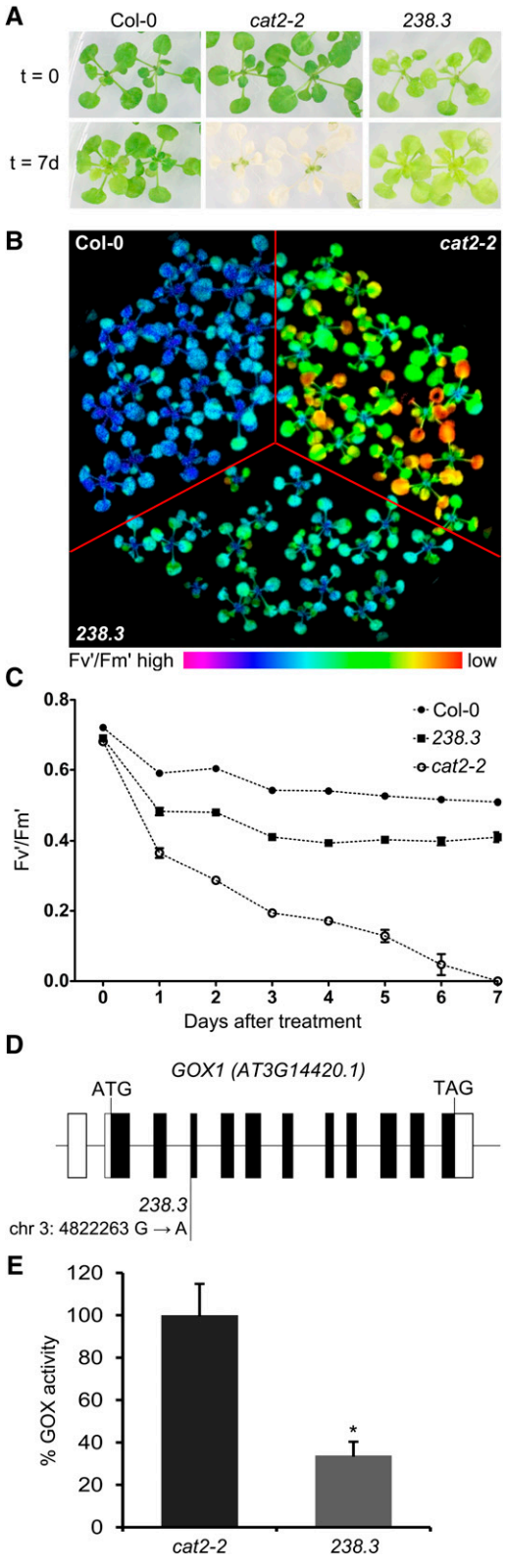

Figure 1. Characterization of line *238.3* that displays attenuated cell death in the absence on peroxisomal catalase under photorespiratory stress. A, Representative bright-field images of 3-week-old Col-0, *cat2-2*, and *238.3* plants before (top panel) and after 7 d (bottom panel) of photorespiratory stress (restricted gas exchange and continuous light). B, Color-coded image of PSII maximum efficiency (Fv′/Fm′) of 3-week-old Col-0, *238.3*, and *cat2-2* plants exposed to photorespiratory stress for 48 h. C, Fv′/Fm′ decrease during the course of the photorespiratory treatment. Data points represent means of three biological replicates ± SE. D, *GOX1* gene model together with the position of the causative EMS-induced mutation. E, Extractable leaf glycolate oxidase activity from 2-week-old plants grown in vitro expressed as a percentage of the *cat2-2* value. Bars represent means of three biological replicates ± SE. Asterisks indicate significant differences according to Student's *t* test (*$P < 0.05$).

genotypes (Fig. 4A). Nevertheless, 608 transcripts responded to the photorespiratory treatment in a genotype-specific manner according to two-factor (genotype and photorespiratory stress) ANOVA (Fig. 4B; Supplemental Data Set 2). In contrast to *cat2-2 gox1-1*, the *cat2-2 gox2-1* transcriptional profile was largely comparable to that of *cat2-2* mutants with only one gene being more responsive to photorespiratory stress (Supplemental Data Set 2). Genes that exhibited higher induction in *cat2-2 gox1-1* in comparison to *cat2-2* mutants were predominantly involved in glycosinolate biosynthesis, jasmonic acid biosynthesis, oxylipin metabolism, and wounding (Supplemental Data Set 3). In contrast, transcripts that were less induced by the photorespiratory treatment in *cat2-2 gox1-1* could be associated with a range of processes such as response to high light, plant-pathogen interaction, salicylic acid-mediated signaling, ethylene biosynthesis, and regulation of programmed cell death (Supplemental Data Set 3).

Parallel analysis of photorespiratory intermediates demonstrated that exposure to photorespiratory stress led to a modest increase (~3-fold) of glycolate in *cat2-2* and Col-0 plants, whereas *cat2-2 gox1-1* and *cat2-2 gox2-1* mutants accumulated 168 and 93 times more glycolate in comparison to their high CO_2-grown controls, respectively (Fig. 5). In contrast, transfer to photorespiration-promoting conditions boosted the Gly (~20-fold) and Ser (~3-fold) content to a comparable level in all genotypes (Fig. 5). Although the steady-state glycerate levels were elevated in all genotypes, its content was higher in *cat2-2 gox1-1* and *cat2-2 gox2-1* double mutants (Fig. 5). Photorespiratory treatment increased the hydroxypyruvate content approximately 3-fold in *cat2-2 gox1-1* and *cat2-2 gox2-1* mutants, while it did not affect Col-0 and *cat2-2* (Fig. 5).

Taken together, these results suggest that the lack of either GOX1 or GOX2 results in inability to process photorespiratory glycolate in a catalase-deficient background. However, the effect is much more pronounced in the absence of GOX1 and *cat2-2 gox1-1* mutants accumulate nearly 2 times more glycolate than *cat2-2 gox2-1* mutants.

Redox Homeostasis in *cat2-2 gox1-1* and *cat2-2 gox2-1* Mutants under Photorespiration-Promoting Conditions

GOX activity is the primary source of H_2O_2 production in photosynthesizing tissues (Noctor et al., 2002). Decreased GOX activity thus might limit H_2O_2 accumulation

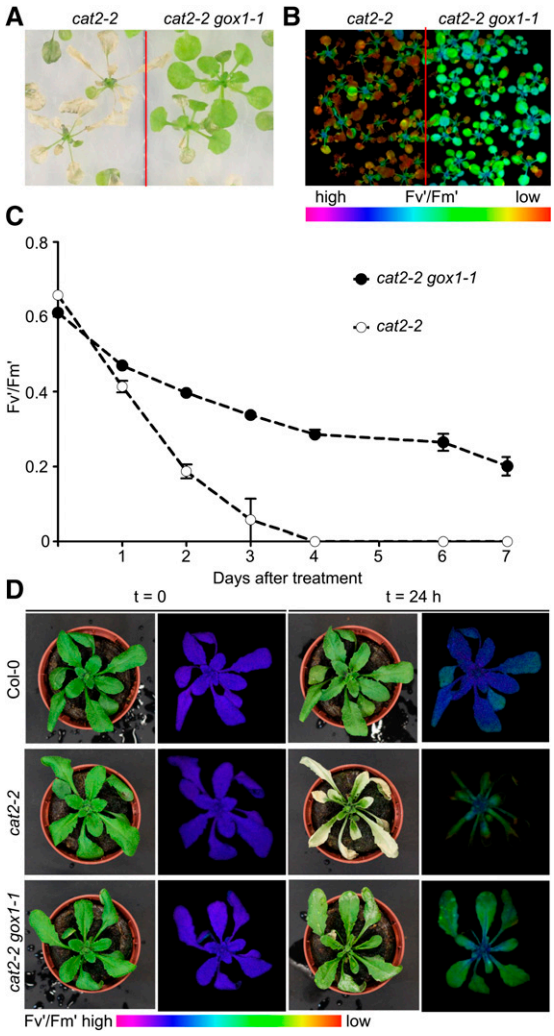

Figure 2. Attenuation of the photorespiratory phenotype of *cat2-2* mutants in the absence of GOX1. A, Representative bright-field image of 3-week-old in vitro-grown *cat2-2* and *cat2-2 gox1-1* mutant plants exposed to photorespiratory stress for 4 d (restricted gas exchange and continuous light). B, Color-coded Fv′/Fm′ images of plants exposed to photorespiratory stress for 48 h. C, PSII maximum efficiency (Fv′/Fm′) decrease in the course of the photorespiratory treatment. Data points represent means of three biological replicates ± SE. D, Representative bright-field and color-coded Fv′/Fm′ images of 3-week-old Col-0, *cat2-2*, and *cat2-2 gox1-1* plants grown in soil under high CO_2 (3,000 μL L^{-1}) atmosphere and low light (100 μmol m^{-2} s^{-1}) before (T=0 h) and after (T=24 h) transfer to ambient air and high light (1,000 μmol m^{-2} s^{-1}).

and attenuate photorespiration-induced cell death in the absence of peroxisomal catalase. Therefore, we assessed the impact of photorespiration-promoting conditions on a common set of differentially regulated genes retrieved from six microarray studies featuring various ROS generating conditions (Willems et al., 2016; see "Materials and Methods"). This ROS-induced transcriptome imprint comprises 322 genes, which are robustly regulated upon perturbation of the redox homeostasis, and was used here as a proxy for H_2O_2 accumulation. The majority of these transcripts responded upon transfer from high CO_2 to photorespiratory stress (high light and ambient air) in all tested genotypes (*cat2-2 gox1-1*, *cat2-2 gox2-1*, and *cat2-2*; Fig. 6). However, the abundance of 48 transcripts was significantly lower in *cat2-2 gox1-1* mutants (Fig. 6), implying an impaired H_2O_2 production and a more stringent regulation of the redox homeostasis.

We further assessed whether the absence of GOX1 could similarly affect the redox poise by quantifying the key redox buffer glutathione/glutathione disulfide (GSH/GSSG) and in situ visualization of H_2O_2 levels with 3,3′-diaminobenzidine (DAB). In 3-week-old plants grown continuously under ambient air, the total glutathione pool in *cat2-2* rosette leaves was significantly larger and more oxidized in comparison to the wild type. Whereas the introduction of *gox2-1* in *cat2-2* background did not alter the total glutathione content and its oxidation status, *cat2-2 gox1-1* mutants accumulated less total glutathione (Supplemental Fig. S4A). In addition, DAB staining revealed an intense signal in *cat2-2* and *cat2-2 gox2-1* mutants, which was largely absent in *cat2-2 gox1-1* mutants and the wild type (Supplemental Fig. S4B).

gox1-1 and *gox2-1* Single Mutants Are Morphologically Indistinguishable under Moderate Light Intensities But, Display Distinct Metabolic Phenotypes

The fact that mutants affected in GOX activity have never been isolated in photorespiratory mutant screens (Timm and Bauwe, 2013), together with the similar enzymatic properties of recombinant GOX1 and GOX2 (Dellero et al., 2015), point toward a strong functional redundancy. Indeed, under moderate light intensities (300 μmol m^{-2} s^{-1}), *gox1-1* and *gox2-1* single mutants were indistinguishable from the wild type and accumulated similar rosette biomass (Fig. 7, A and B), despite displaying only half of the wild-type foliar GOX activity (Fig. 7C). In contrast, under such growth conditions, *cat2-2* and *cat2-2 gox2-1* mutants were stunted and developed leaf lesions. Both of these phenotypes were largely abolished in *cat2-2 gox1-1* mutants (Fig. 7A). Interestingly, GOX activity from *cat2-2* leaves was comparable to that extracted from single *gox* mutants (Fig. 7C). Introduction of *gox1-1* or *gox2-1* into the *cat2-2* background further reduced leaf GOX activity to levels below those found in single *cat2-2* mutants (Fig. 7C).

We further tested whether, despite the lack of growth phenotype, the low foliar GOX activity found in *gox1-1* and *gox2-1* mutants affected the steady-state levels of photorespiratory metabolites. Interestingly, *gox1-1* mutants accumulated more glycolate (3.7-fold) than *gox2-1* mutants (1.3-fold) relative to the wild type (Fig. 8). Moreover, *cat2-2 gox1-1* and *cat2-2 gox2-1* mutants contained approximately 50 and 5 times more glycolate than the wild type, respectively. Apart from glycerate, which was lower in *gox2-1* single mutants, the levels of the other quantified photorespiratory intermediates (Gly, Ser, and hydroxypyruvate) were similar between *gox1-1*, *gox2-1*, and wild-type plants (Fig. 8).

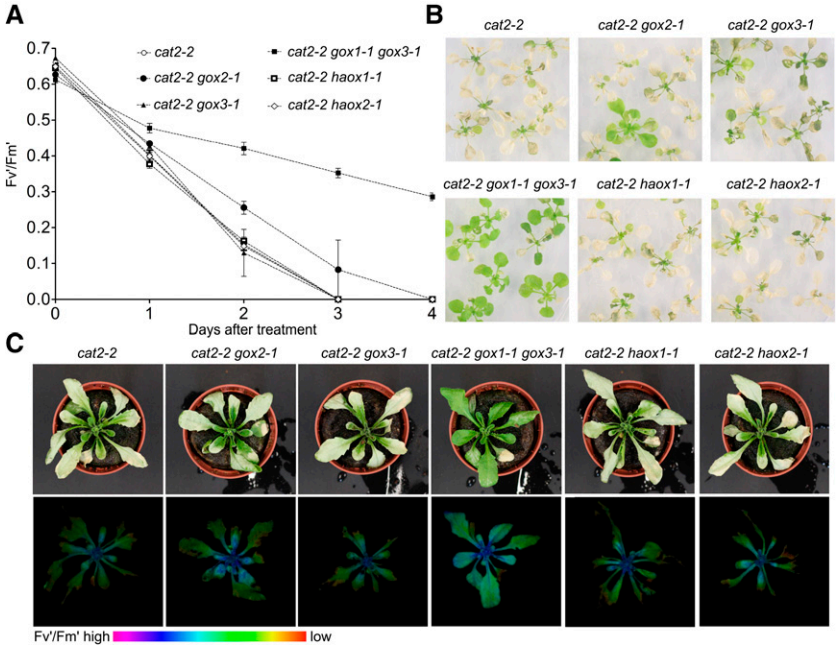

Figure 3. Contribution of (L)-2-hydroxyacid-oxidase family members to the photorespiratory phenotype of *cat2-2* mutants. A, Decrease of PSII maximum efficiency (Fv′/Fm′) in 3-week-old in vitro-grown plants during the course of the photorespiratory stress (restricted gas exchange and continuous light). Data points represent means of three biological replicates ± SE. B, Representative bright-field images of 3-week-old plants exposed photorespiratory stress for 4 d (restricted gas exchange and continuous light). C, Representative bright-field (top panel) and color-coded Fv′/Fm′ (bottom panel) images of 3-week-old plants grown in soil under high CO_2 (3,000 μL L^{-1}) atmosphere and low light (100 μmol m^{-2} s^{-1}) after transfer to ambient air and high light (1,000 μmol m^{-2} s^{-1}) for 24 h.

High Light Conditions Elicit Differential Responses in *gox1-1* and *gox2-1* Mutants

The differential photorespiratory response of *cat2-2 gox1-1* and *cat2-2 gox2-1* double mutants indicates that GOX1 and GOX2 are not entirely redundant. To further deconvolute the individual roles of the two isoforms, 3-week-old *gox1-1* and *gox2-1* mutants grown under light intensities limiting photorespiration (100 μmol m^{-2} s^{-1}), which showed no apparent differences in morphology and photosynthetic light reactions in comparison to the wild type, were exposed to high-intensity blue light (700 μmol m^{-2} s^{-1}) inside an imaging PAM (pulse amplitude modulation), which allowed to follow their photosynthetic performance. Data for steady-state chlorophyll fluorescence (F_s) and maximal fluorescence under light (F_m') were collected over 10 h of

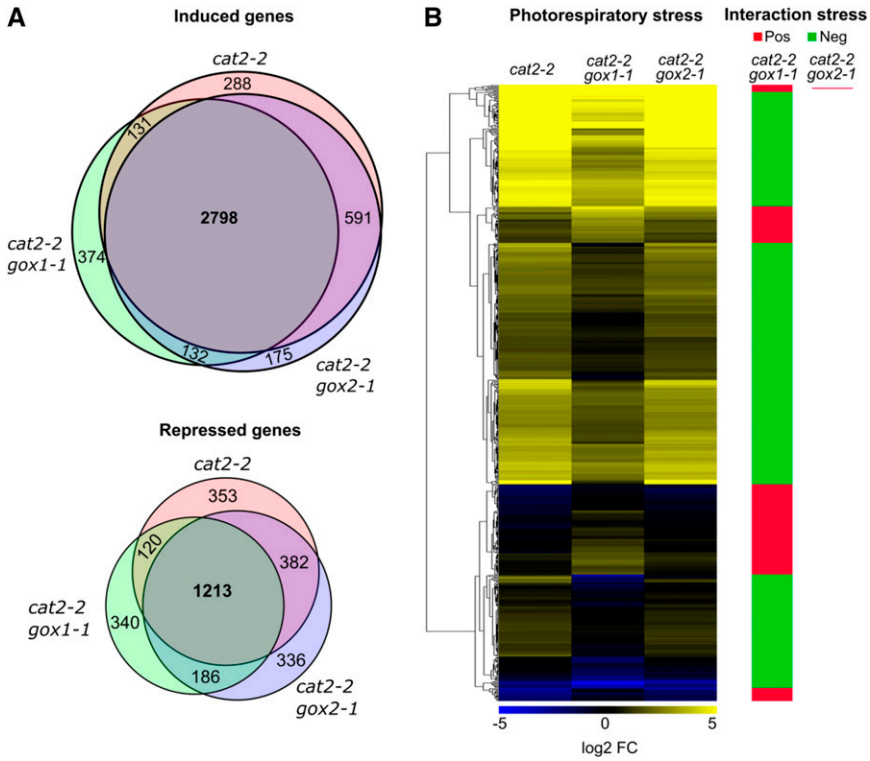

Figure 4. Global transcriptome changes triggered by photorespiratory stress in *cat2-2*, *cat2-2 gox1-1*, and *cat2-2 gox2-1* mutants. Three-week-old plants grown in soil under high CO_2 (3,000 μL L^{-1}) atmosphere and low light (100 μmol m^{-2} s^{-1}) were transferred to ambient air and high light (1,000 μmol m^{-2} s^{-1}) for 3 h. Genome-wide gene expression levels were quantified in mature rosette leaves before and after exposure to photorespiratory stress using RNA-seq. A, Venn diagrams showing the number of induced (top panel) or repressed (bottom panel) transcripts ($|\log_2 FC| > 1$, FDR < 0.01) upon photorespiratory stress. B, Heat map of transcripts that responded significantly (FDR < 0.05) to the photorespiratory stress in a genotype-specific manner according to a two-way ANOVA. Clusters of transcripts with higher or lower expression in the double mutants relative to *cat2-2* mutants are marked with red or green, respectively.

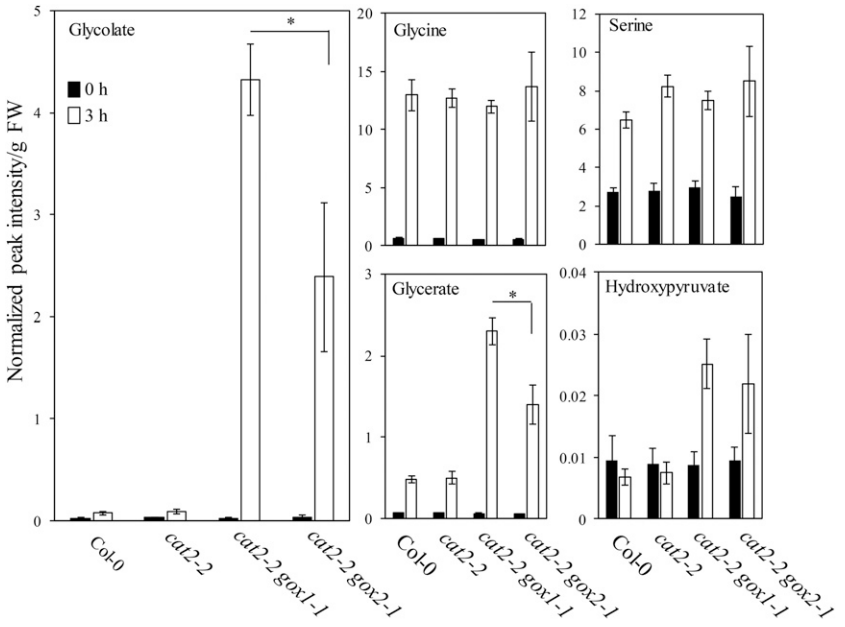

Figure 5. Changes of photorespiratory intermediates triggered by photorespiratory stress. Three-week-old Col-0, *cat2-2*, *cat2-2 gox1-1*, and *cat2-2 gox2-1* plants grown in soil under high CO_2 (3,000 μL L^{-1}) atmosphere and low light (100 μmol m^{-2} s^{-1}) were transferred to ambient air and high light (1,000 μmol m^{-2} s^{-1}) for 3 h. Metabolites were extracted from rosette leaves before (0 h) and after exposure to photorespiratory stress (3 h). Bars represents averages of 5 to 6 replicates ± SD. Data were analyzed with two-way ANOVA using photorespiratory stress (photorespiratory conditions versus control conditions) and genotype as main factors. Asterisks indicate significant differences between genotypes under photorespiratory stress ($P < 0.05$).

exposure to high light and used to calculate the apparent rate of electron transfer (ETR) through PSII and nonphotochemical quenching (NPQ). Initially, high light exposure negatively affected the ETR through PSII in both *gox1-1* and *gox2-1* mutants in comparison to the wild type (Fig. 9A). However, after 2 h of high light treatment, ETR started to recover. The recovery was more pronounced in *gox2-1* mutants and they eventually reached wild-type ETR levels, whereas *gox1-1* mutants did not fully recover. The high light treatment increased the NPQ levels in both *gox1-1* and *gox2-1* mutants above those recorded for the wild type (Supplemental Fig. S5A).

To explore the underlying reason for the diminished ETR and increased NPQ in both *gox* lines, we collected maximal quantum yield of PSII (F_v/F_m) data over time by subjecting the plants to consecutive periods of high-intensity blue light (900 μmol m^{-2} s^{-1}) and darkness (see "Materials and Methods"). Such treatment negatively affected the F_v/F_m ratio, indicative for PSII photoinhibition, in all tested genotypes, but the decline was especially pronounced in *gox1-1* and *gox2-1* single

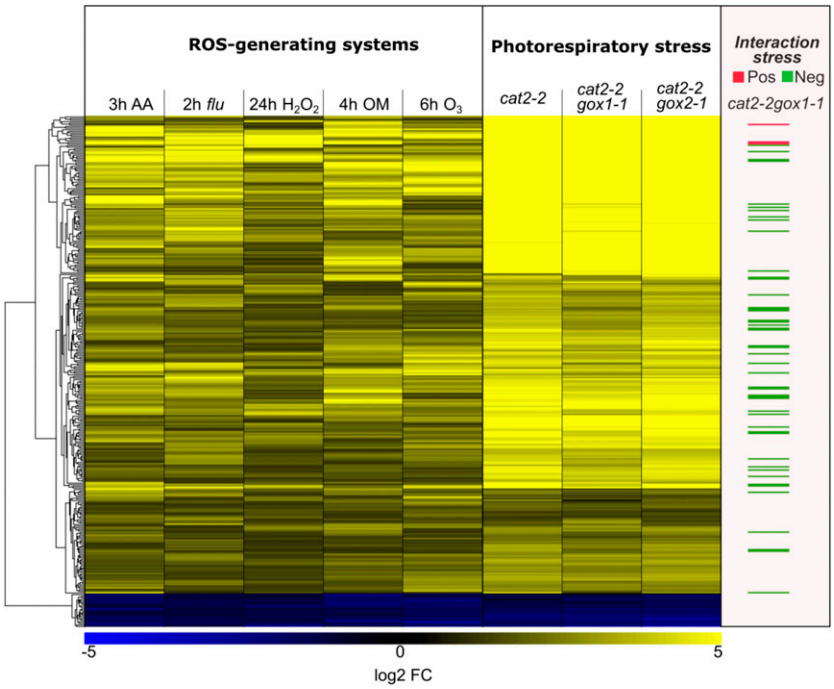

Figure 6. Cellular redox homeostasis upon exposure to photorespiratory stress in *cat2-2*, *cat2-2 gox1-1*, and *cat2-2 gox2-1* mutants. Comparison between the expression patterns of a subset of ROS-responsive genes, obtained by meta-analysis of ROS-generating systems, found in the transcriptome signatures of *cat2-2*, *cat2-2 gox1-1*, and *cat2-2 gox2-1* mutants. The following experiments were used in the meta-analysis: reillumination of the conditional *flu* mutant for 2 h after a dark acclimation (2 h *flu*, GSE10812); treatment of seedlings with oligomycin for 4 h (4 h OM, GSE38965); treatment of seedlings with 50 μM antimycin A for 3 h (3 h AA, GSE41136); exposure of seedlings to ozone for 6 h (6 h O_3, E-MEXP-342); treatment of seedlings with 10 mM H_2O_2 for 24 h (24 h H_2O_2).

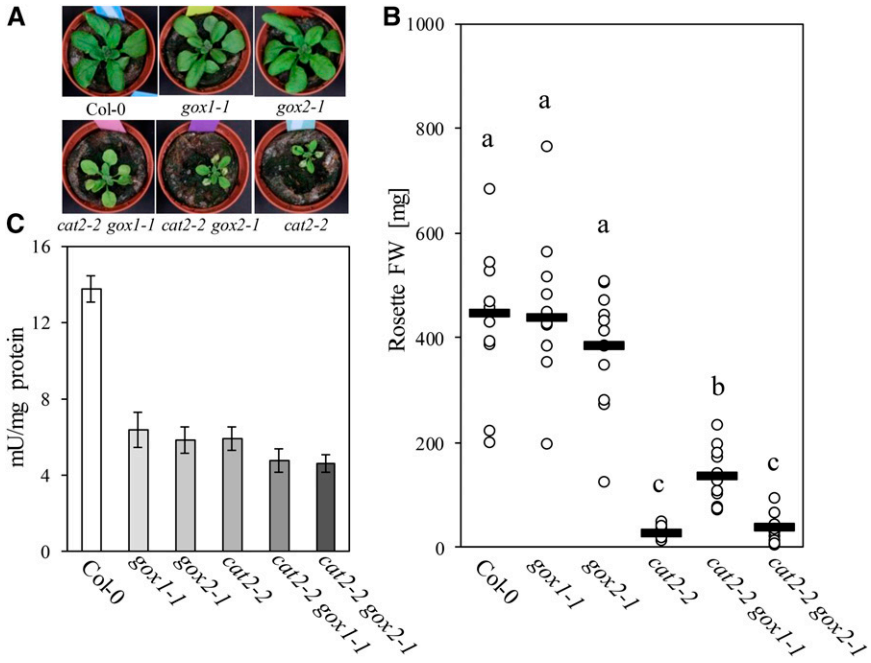

Figure 7. Phenotypic characteristics of Col-0, *gox1-1*, *gox2-1*, *cat2-2*, *cat2-2 gox1-1*, and *cat2-2 gox2-1* plants grown under moderate light intensity (300 μmol m^{-2} s^{-1}). A, Representative bright-field images of 3-week-old plants. B, Rosette fresh weight (FW) of 3-week-old plants. Black lines represent medians from at least 10 replicates and dots individual measurements. Different letters denote homogenous subsets according to a one-way ANOVA with Tukey post hoc test. C, Extractable leaf GOX activity from 3-week-old plants. Bars represent averages from three biological replicates ± SD.

mutants (Fig. 9B). Both mutants entered the recovery phase simultaneously; however, the recovery rate was significantly higher in *gox2-1* than in *gox1-1*. Moreover, *gox2-1* mutants nearly reached wild-type F_v/F_m levels by the end of the treatment. These findings suggest that the most likely explanation for the transient drop in ETR upon exposure to continuous high-intensity blue light is inhibition of PSII activity.

To probe whether the PSII photoinhibition observed in the *gox* mutants exposed to high light is accompanied with an altered redox status of the plastoquinone pool, the phosphorylation state of light-harvesting antennae of PSII (LHCBII) was assessed with an anti-phospho-Thr antibody. Overreduction of the plastoquinone pool activates the thylakoid-associated kinase STN7 that phosphorylates LHCBII, thereby increasing their affinity to PSI (Rochaix, 2014). The exposure to high light led to a time-dependent dephosphorylation of LHCBII in all tested genotypes, pointing toward a uniform impact on the plastoquinone pool (Supplemental Fig. S5B).

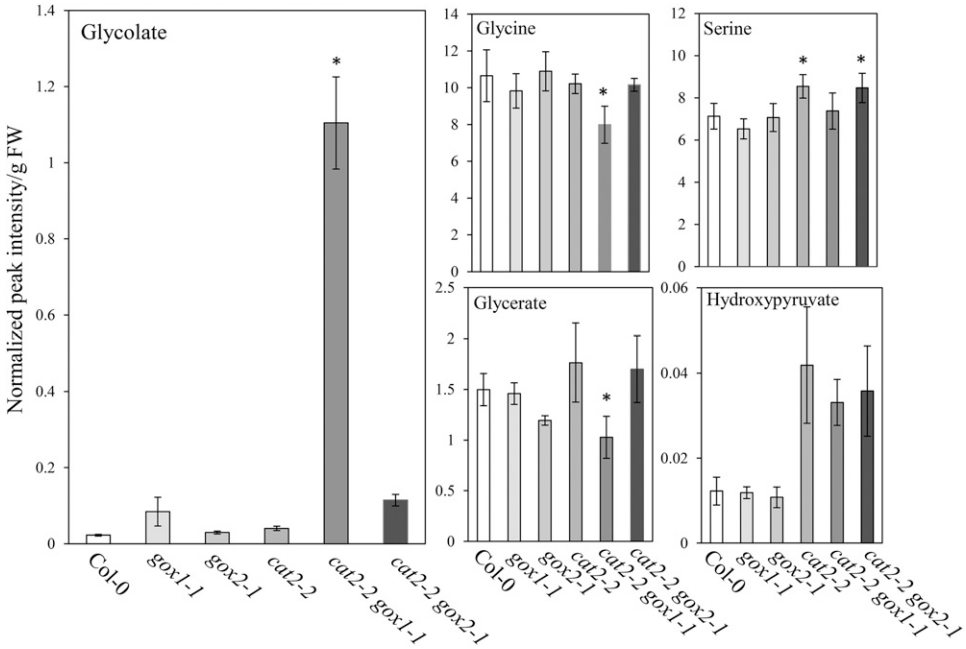

Figure 8. Levels of photorespiratory intermediates in rosettes of Col-0, *gox1-1*, *gox2-1*, *cat2-2*, *cat2-2 gox1-1*, and *cat2-2 gox2-1* plants grown under moderate light intensity (300 μmol m^{-2} s^{-1}). Bars represents averages of 5 to 6 replicates ± SD. Asterisks indicate significant differences ($P < 0.05$) in comparison to Col-0 according to one-way ANOVA and Tukey post hoc test.

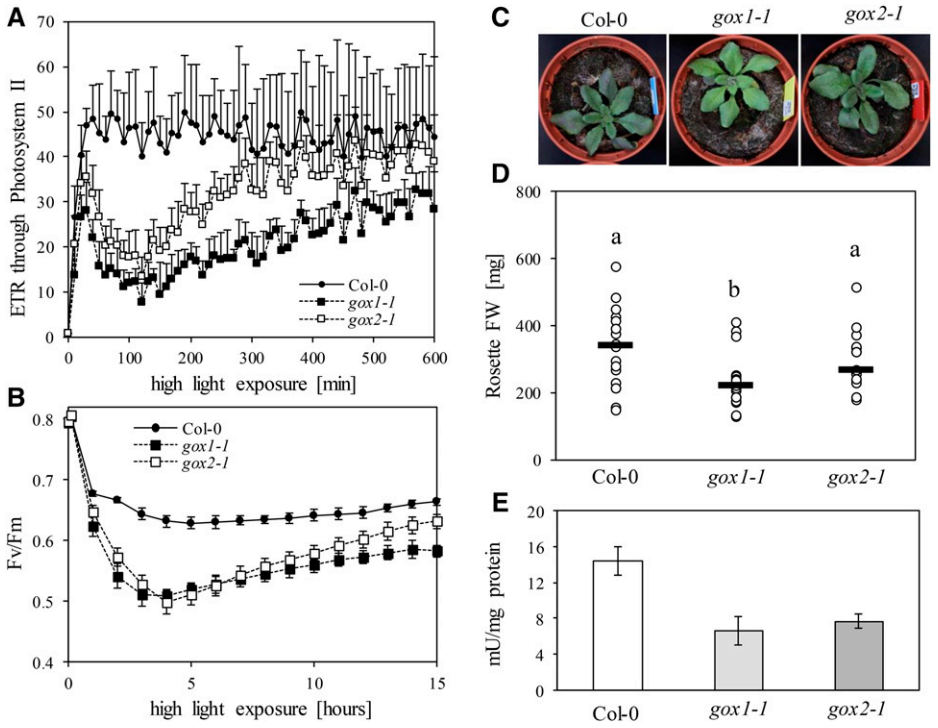

Figure 9. Phenotypic characteristics of Col-0, *gox1-1*, and *gox2-1* single mutants under high light. A and B, Changes in photosynthetic electron transfer reactions after shift from a nonphotorespiratory growth environment to high light. Changes in apparent ETR through PSII (A) and maximal quantum yield of PSII (F_v/F_m; B) are plotted against the incubation time under high light. C, Representative bright-field images of 3-week-old plants grown under high light intensities (1,000 μmol m^{-2} s^{-1}). D, Rosette biomass of 3-week-old plants grown under high light intensities (1,000 μmol m^{-2} s^{-1}). Black lines represent medians from at least 15 replicates and dots individual measurements. Different letters denote statistical differences according to a one-way ANOVA with Tukey post hoc test. E, Extractable leaf GOX activity from 3-week-old plants grown under high light intensities (1000 μmol m^{-2} s^{-1}). Bars represent averages from three biological replicates ± SD.

To further corroborate specific functionalities for GOX1 and GOX2, we grew *gox1-1* and *gox2-1* mutants under high light intensity (~1,000 μmol m^{-2} s^{-1}). Under these conditions, *gox1-1* mutants accumulated less rosette biomass than *gox2-1* mutants, whereas both *gox1-1* and *gox2-1* were smaller than the wild type (Fig. 9, C and D). The foliar GOX activity was similar in both mutants and nearly half of that found in the wild type (Fig. 9E). The lower biomass of *gox1-1* mutants correlated with elevated glycolate levels (~18-fold) relative to the wild type (Fig. 10). In contrast, the glycolate content of *gox2-1* mutants was not significantly different from that of the wild type. Similarly to glycolate, Gly and glycerate levels were elevated in *gox1-1*, but not in *gox2-1* mutants under these growth conditions (Fig. 10).

Evolutionary Analysis of *GOX1* and *GOX2*

To further investigate the origin and evolution of the two highly similar protein-coding *GOX1* and *GOX2* sequences in Arabidopsis, we selected their orthologs in close relatives based on conserved synteny blocks that flank *GOX1* and *GOX2* (Louis et al., 2015). *GOX1* and *GOX2* are present as "tandem" duplicates in all Brassicaceae species with the exception of *Arabidopsis lyrata*, which retained only *GOX1* (Fig. 11A). The only other plant species for which statistically significant colinearity or synteny could be found (our criterion to decide on true orthology) were the Solanaceae species *Solanum tuberosum* and *Solanum lycopersicum*, which contain only one *GOX* gene (Fig. 11A). This, together with the fact that *GOX1* and *GOX2* genes in Brassicaceae form a monophyletic cluster when compared with genes from more close relatives (Supplemental Fig. S6), would suggest that the tandem duplication that gave rise to *GOX1* and *GOX2* occurred in the most recent common ancestor of the Brassicaceae and is therefore Brassicaceae specific.

Using the *GOX1* and *GOX2* orthologs, we tested whether they had experienced different selection forces during their evolutionary history following the duplication event. Such differences might explain the different phenotypes observed in single *gox1-1* and *gox2-1* mutants. To this end, we estimated the ratio of nonsynonymous substitutions rates to synonymous substitution rates (ω) over time using the branch models implemented in PAML (Yang, 2007). We further reconstructed a maximum likelihood tree based on amino acid sequences (see "Materials and Methods") that also reflected the duplication event prior to the divergence of Brassicaceae (Fig. 11B). In a three-ratio model using the Solanaceae gene clade as a background, the obtained ω values for the *GOX1* and *GOX2* clades were 0.064 and 0.104, respectively. Both of them were higher than the ω value for the Solanaceae clade: 0.038. The three-ratio model was significantly better than a one-ratio model with one ω value for all three clades ($2\Delta\ell$ = 18.4962; df = 2; $P = 9.63\ E^{-5}$), which implies that the *GOX1* and *GOX2* clades experienced different selection forces following duplication.

Because most Brassicaceae have retained both *GOX1* and *GOX2* genes (Fig. 11A), different selection pressures might have acted in both postduplication branches

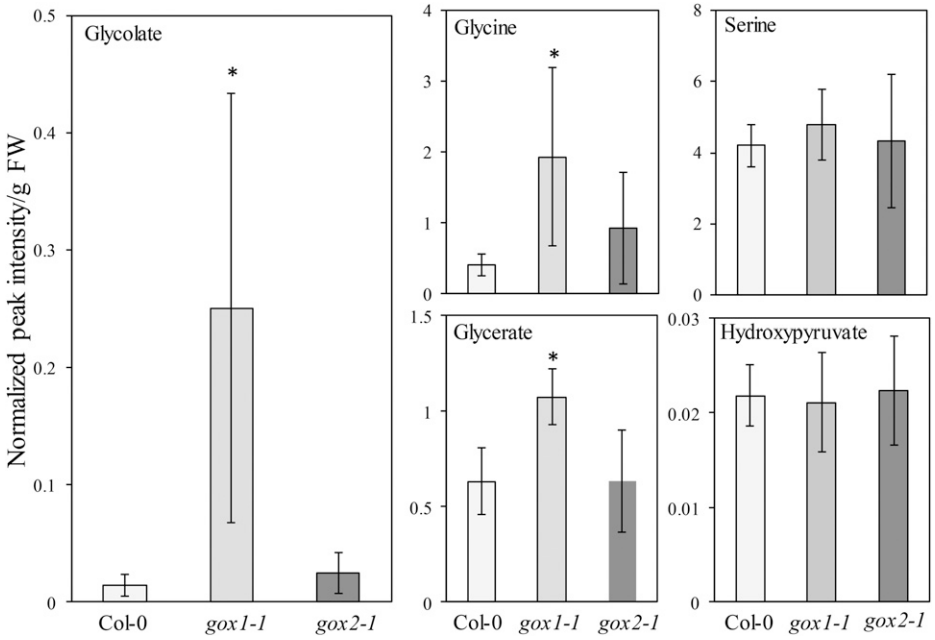

Figure 10. Levels of photorespiratory intermediates in rosettes of 3-week-old Col-0, *gox1-1*, and *gox2-1* plants grown under high light intensity (1,000 μmol m^{-2} s^{-1}). Bars represent averages of 5 to 6 replicates ± SD. Asterisks indicate significant difference ($P < 0.05$) in comparison to Col-0 according to one-way ANOVA with Tukey post hoc test.

before the divergence of the Brassicaceae. We thus compared ω values on the two postduplication branches, indicated by arrows in Figure 11B, using the rest of the branches as a background (Supplemental Tables S1 and S2). Apparently, both early postduplication branches underwent purifying selection with an ω value significantly less than 1 ($P = 0.02$, D–H in Supplemental Table S2). The ω value for the branch leading to the *GOX1* clade was indistinguishable from the background ($P = 0.16$ for A–C and $P = 0.57$ for B–E in Supplemental Table S2), whereas the one leading to the *GOX2* clade was significantly higher than the background ($P = 0.001$ for A and B and $P = 0.003$ for C–E in Supplemental Table S2), but not significantly over 1 ($P = 0.67$, E–I in Supplemental Table S2). To further examine whether positive selection acted on *GOX2* in Arabidopsis, we carried out PAML with the modified branch-site model (Zhang et al., 2005). No signal of positive selection was detected (Supplemental Table S3).

Our evolutionary analysis implies that although both *GOX1* and *GOX2* underwent purifying selection following their duplication, *GOX2* did experience a more relaxed selection pressure than *GOX1*, which might underlie the differential phenotypes observed in single *gox1-1* and *gox2-1* mutants.

DISCUSSION

In contrast to the majority of the photorespiratory enzymes, *gox* mutants have never been isolated in photorespiratory mutant screens pointing toward a genetic redundancy among the GOX family members (Timm and Bauwe, 2013). Indeed, the Arabidopsis genome contains five genes annotated as glycolate oxidases (*GOX1*, *GOX2*, *GOX3*, *HAOX1*, and *HAOX2*). The data presented here provide new insights into the GOX functional redundancy and reveal distinct functions for the photorespiratory GOX isoforms in Arabidopsis.

In a second-site suppressor screen, we identified a causative loss-of-function mutation in the gene encoding GOX1 that attenuated the photorespiratory phenotype of Arabidopsis mutants lacking peroxisomal catalase. Interestingly, the highly similar GOX2 did not alleviate the photorespiratory phenotype of *cat2-2* mutants, implying that GOX1 and GOX2 are functionally nonidentical. The absence of none of the other Arabidopsis enzymes predicted to metabolize glycolate could not counteract the characteristic photosynthetic decline and cell death observed in *cat2-2* mutants exposed to photorespiratory stress (Fig. 3). This could be largely explained by their substrate specificities and expression patterns. HAOX1 and HAOX2 preferentially metabolize medium- and long-chain hydroxyacids (Esser et al., 2014), and their absence did not significantly affect the extractable leaf GOX activity (Supplemental Fig. S7). Similarly, the lack of GOX3, which is predominantly expressed in roots and senescing leaves and uses glycolate and L-lactate with comparable efficiency (Engqvist et al., 2015), did not reduce the GOX activity (Supplemental Fig. S7). Interestingly, *haox1-1*, *haox2-1*, and *gox3-1* mutants have been previously reported to possess only 30% of the wild-type GOX activity (Rojas et al., 2012). The discrepancy with our results, which revealed no differences in GOX activity between *haox1-1*, *haox2-1*, and *gox3-1* mutants and the wild type, might be explained by plant age and growth conditions.

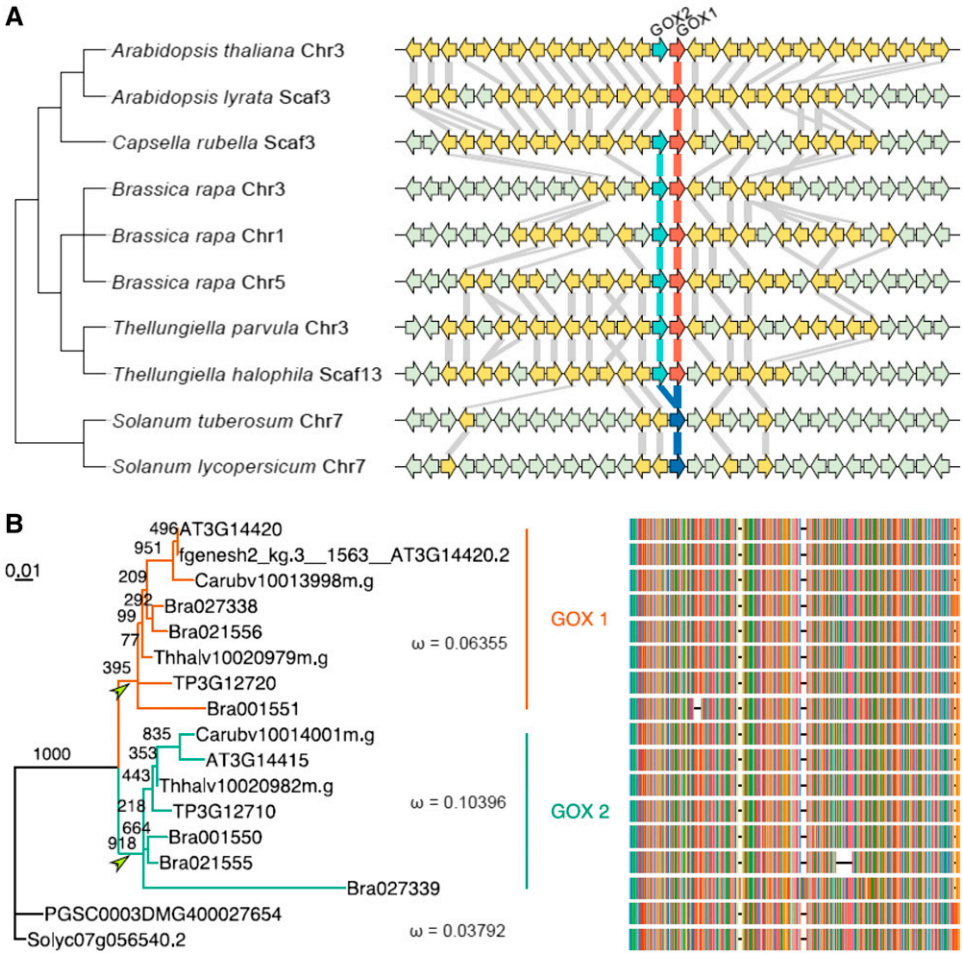

Figure 11. Evolutionary analysis of *GOX1* and *GOX2*. A, Conserved synteny surrounding *GOX1* and *GOX2* as retrieved from Genomicus (v16.03) and visualized with genoPlotR. Arrowed blocks indicate genes, with yellow and gray denoting homologous and nonhomologous genes to Arabidopsis, respectively. Red and green arrows indicate *GOX1* and *GOX2* in Brassicaceae, respectively, and blue arrows are *GOX* genes in Solanaceae. Gray lines connect homologous genes between neighbors in the tree. Chromosome or scaffold numbers on which the conserved synteny blocks were found are also indicated. B, Unrooted maximum likelihood tree and multiple sequence alignment for GOX genes. The numbers along branches show bootstrap support. Green and red indicate the *GOX1* and *GOX2* clade, respectively. Two arrowheads denote two postduplication branches. ω is the ratio of the nonsynonymous substitution rate over the synonymous substitution rate for the indicated clades as calculated with PAML under a three-ratio model.

The photorespiratory GOX activity produces approximately 70% of the total H_2O_2 pool and is thus the most important H_2O_2 source in photosynthesizing C3 leaves (Noctor et al., 2002). The absence of peroxisomal catalase (CAT2) in *cat2-2* mutants results in perturbed redox homeostasis and cell death formation under photorespiration-promoting conditions (Queval et al., 2007). Given that the majority of H_2O_2 in photosynthesizing leaves is generated by the GOX activity, the most straightforward explanation for the alleviated photorespiratory phenotype of *cat2-2* mutants in the absence of GOX is a limited H_2O_2 production. This assumption implies that GOX1 and GOX2 are functionally divergent and that GOX1 produces more H_2O_2, thus explaining the alleviated cell death of *cat2-2 gox1-1* but not *cat2-2 gox2-1* mutants. Indeed, DAB staining indicated lower H_2O_2 levels in *cat2-2 gox1-1* mutants in comparison to *cat2-2 gox2-1* and *cat2-2* mutants, which were accompanied with a more stringent regulation of glutathione homeostasis and higher accumulation of glycolate (Supplemental Fig. S4A; Fig. 8). Moreover, ROS-related transcripts were less induced in *cat2-2 gox1-1* mutants in comparison to *cat2-2* and *cat2-2 gox2-1* mutants, which were largely identical. Taken together, these results reveal that the seemingly redundant GOX1 and GOX2 are not identical and the H_2O_2 levels produced by the residual GOX1 in *cat2-2 gox2-1* mutants are sufficient to trigger cell death under photorespiration-promoting conditions.

Activation of antioxidant systems that can compensate for the lack of CAT2 and scavenge excess H_2O_2 could also underlie the alleviated cell death of *cat2-2 gox1-1* mutants. Ascorbate peroxidases (APXs) are key enzymes in the ascorbate-glutathione cycle that remove H_2O_2 using ascorbate as an electron donor (Dietz, 2016). Nine APX isoforms distributed between chloroplasts, mitochondria, cytosol, and microsomes, including peroxisomes, have been described in Arabidopsis (Mittler et al., 2004). APX transcripts levels are responsive to adverse environmental conditions and total APX activity generally increases under stress (Caverzan et al., 2012). Knocking out the most abundant cytosolic and chloroplastic APXs negatively affects plant growth, development, and susceptibility to stresses, such as high light (Pnueli et al., 2003; Maruta et al., 2010). In contrast, *apx3* mutants lacking peroxisomal APX are phenotypically not affected under optimal or stress conditions (Narendra et al., 2006). The transcript

abundance of the H_2O_2-responsive cytosolic *APX2* was lower in *cat2-2 gox1-1* mutants, whereas *APX1*, another cytosolic isoform, was slightly more induced in comparison to *cat2-2* and *cat2-2 gox2-1* mutants (Supplemental Data Set 2). The absence of APX1 results in H_2O_2 accumulation and degradation of the chloroplastic antioxidant machinery under moderate light intensities, suggesting a protective role of the cytosol on the chloroplast function (Davletova et al., 2005). The moderate induction of *APX1* in *cat2-2 gox1-1* mutants might therefore contribute to the alleviated cell death phenotype in the absence of peroxisomal catalase.

Functional catalase is crucial for the protection of GOX, which is highly susceptible to oxidative damage (Schäfer and Feierabend, 2000). In support of this notion, we found that the leaf GOX activity in *cat2-2* mutants is significantly lower than in the wild type (Fig. 7). The low GOX activity observed in *cat2-2* mutants can be attributed to the preventive role played by the peroxisomal catalase in limiting the degradation of the redox vulnerable GOX cofactor FMN which in its reduced form ($FMNH_2$) contributes to ROS generation (Massey, 1994). Chemically inhibiting catalase with 3-amino-1,2,4-triazole, similarly to the *cat2-2* mutation, negatively affects GOX activity (Schäfer and Feierabend, 2000). The crucial role of catalase in maintaining GOX activity seems to be also dependent on the presence of GSH because pharmacologically blocking GSH biosynthesis inactivated GOX even in the presence of catalase (Schäfer and Feierabend, 2000). Both GOX1 and GOX2 have a single, highly conserved Cys residue (Proost et al., 2015) that potentially could serve as a site for redox-dependent posttranslational modification governing protein function and stability under oxidative conditions. The redox activity of the Cys residue was corroborated by Rouhier et al. (2005) who isolated GOX1 following affinity chromatography purification with poplar GLUTAREDOXIN C4, indicating that it could be subjected to *S*-glutathionylation. Moreover, GOX from *Kalanchoe pinnata* (Abat et al., 2008) and *Pisum sativum* (Ortega-Galisteo et al., 2012) were described as targets for S-nitrosylation.

Mutants lacking GOX1 and GOX2 have been previously shown to be morphologically and metabolically indistinguishable from wild-type plants under light intensity of 200 μmol m^{-2} s^{-1}, implying a redundant role for both isoforms (Dellero et al., 2016). Similarly, under our experimental conditions, light intensity of 300 μmol m^{-2} s^{-1} did not provoke any visible difference between single *gox1-1* and *gox2-1* mutants and the wild type. However, we observed a trend toward increased glycolate levels in the absence of GOX1 (Fig. 8), suggesting the existence of distinct metabolic roles for GOX1 and GOX2. Indeed, when grown under higher light intensities (1,000 μmol m^{-2} s^{-1}), *gox1-1* mutants accumulated nearly 18 times more glycolate than *gox2-1* mutants and the wild type (Fig. 10). The functional difference between the two isoforms is further supported by the faster PSII recovery rate observed in *gox2-1* mutants under high light in comparison to *gox1-1* (Fig. 9A). Nevertheless, both *gox1-1* and *gox2-1* mutants displayed similar initial rates of PSII photodamage upon exposure to high light (Fig. 9A; Supplemental Fig. S5), implying that the abrupt increase in photosynthetic electron flow against the background of restricted photorespiratory pathway creates similar imbalance in electron transfer chains. This notion is further supported by the increased phosphorylation of LHCBII in both mutant lines in comparison to the wild type (Supplemental Fig. S5), which is indicative of overreduction of the plastoquinone pool. The predominant metabolic role of GOX1 evident from the above described experiments is also substantiated by the higher transcriptional abundance of *GOX1* (Supplemental Fig. S8; Dellero et al., 2016). The transcriptional differences, however, were not reflected in the extractable leaf GOX activity (Fig. 7). Thus, it would be important to quantitatively evaluate the individual GOX isoforms at the protein level. The *gox1-1* mutants are only slightly affected under high light, suggesting that the residual GOX2 can partially compensate for the loss of GOX1. Only the simultaneous knock down of GOX1 and GOX2 by artificial microRNA, which results in 5% residual GOX activity, leads to a severely stunted growth phenotype (Dellero et al., 2016).

The duplication event that gave rise to *GOX1* and *GOX2* occurred before the divergence of Brassicaceae, which has been dated approximately 40 million years ago (Bailey et al., 2006). The high similarity of the two genes suggests that both of them have been under a purifying selection, which minimized the generation of deleterious mutations in their coding sequences, for the last 40 million years. However, our evolutionary analysis revealed more relaxed selection pressure on *GOX2* that might underlie the differential phenotypes observed in the absence of GOX2. Although the differences might be due to a positive selection acting on a few sites, the branch-site model did not support this hypothesis. The relaxed purifying selection on *GOX2* was also reflected in the evolutionary forces acting on the six *GOX* paralogs from *Brassica rapa* that originated in the well-documented paleohexaploidization (Wang et al., 2011). Not only four of the six genes have already started degrading, but also two *GOX2* paralogs accumulated larger insertions and deletions in comparison to the *GOX1* paralogs (Fig. 11B). This is in accordance with the different ω values for the two ancestral branches and the loss of *GOX2* from a conserved synteny block in *A. lyrata*, which together support a major role for GOX1 in photorespiratory metabolism.

In conclusion, our results provide evidence for distinct roles of the two photorespiratory GOX isoforms in Arabidopsis. Lack of GOX1, but not GOX2, attenuates the cell death phenotype of *cat2-2* mutants under photorespiratory conditions. This is accompanied by higher levels of accumulated glycolate in the absence of GOX1, suggesting that under conditions promoting photorespiration, GOX1 is the isoform that predominantly metabolizes glycolate and produces H_2O_2.

MATERIALS AND METHODS

Plant Material

All mutants used in this study are in the Col-0 background and were described before: *cat2-2* (Queval et al., 2007); *gox1-1*, *gox2-1*, *gox3-1*, *haox1-1*, *haox2-1*, and *gox1-1 gox3-1* (Rojas et al., 2012). Double and triple knockout lines *cat2-2 gox1-1*, *cat2-2 gox2-1*, *cat2-2 gox3-1*, *cat2-2 haox1-1*, *cat2-2 haox2-1*, and *cat2-2 gox1-1 gox3-1* were generated by crossing *cat2-2* plants (pollen acceptors) with the respective mutant lines (pollen donors). Double mutant plants were identified in F2 segregating populations by PCR genotyping with respective primers (Supplemental Table S4).

Growth Conditions and Stress Treatments

To impose photorespiratory stress in vitro, seeds were surfaced-sterilized by fumigation and cold-treated at 4°C for 3 to 4 d. Plants were germinated and grown on full-strength Murashige and Skoog (MS) medium (1% [w/v] Suc and 0.8% [w/v] agar) under controlled environmental conditions (16 h/8 h light/dark, 100 μmol m^{-2} s^{-1} light intensity, 21°C). After 3 weeks, plates were sealed with multiple layers of Parafilm M (Bemis Flexible Packaging) in order to reduce gas exchange and transferred to continuous light (100 μmol m^{-2} s^{-1} light intensity, 21°C). Data for PSII maximum efficiency (Fv′/Fm′) were recorded daily using an Imaging-PAM-Series chlorophyll fluorescence system (Heinz Walz).

To impose severe photorespiration, plants were initially germinated in soil and grown under high CO_2 atmosphere (3000 μL L^{-1}) in a controlled climate chamber (Vötsch Industrietechnik; 16 h/8 h light/dark, 21°C, 50% relative humidity). Three-week-old plants were transferred to high light (~1,000 μmol m^{-2} s^{-1}) and ambient air for the specified time periods.

To investigate the effect of light intensity, plants were grown in soil under long-day conditions (16 h/8 h light/dark) in a controlled climate chamber (Sanyo Fitotron; 21°C and 50% relative humidity). Light intensity was set to either 300 or 1000 μmol m^{-2} s^{-1}.

Identification of a Causative Mutation in *238.3*

In order to identify the causative mutation of line *238.3*, we applied the SHOREmap backcross pipeline (Hartwig et al., 2012). For this, we analyzed an F2 mapping population derived from a cross between *cat2-2* and *238.3* mutant lines. In total, 1,794 F2 individuals were subjected to photorespiratory assay conditions in vitro and about 13% of plants (234) exhibited reversion of the cell death phenotype. This segregation did not fit the Mendelian 1:3 ratio (χ^2 = 137.319, $P < 0.0001$) presumably due to the limited penetrance of the revertant phenotype and/or presence of independent EMS-induced mutations negatively affecting the seedling performance. Surviving plants were harvested and used for preparation of nuclear DNA (Schneeberger et al., 2009). This sample was used to prepare an Illumina library, which was sequenced to an average 53.6-fold genome coverage. Backcrossing of a mutant to its parent line does not introduce prespecified markers into the mapping population. Therefore, we applied a SHOREmap backcross strategy (Hartwig et al., 2012) that uses EMS-induced markers as novel markers in order to determine the mapping interval. Using a concordance threshold set to 0.8, we identified 10 EMS-specific SNPs (Supplemental Table S5) significantly enriched in plants displaying a revertant phenotype. All polymorphisms localized to the upper arm of chromosome 3 within 3.3 to 7.4 Mb physical interval. The most frequent SNP was localized within the *GOX1* (At3g14420) coding sequence at position 1 of the third exon. Analysis of the *GOX1* mutant sequence performed with NetGene2 software (http://www.cbs.dtu.dk/services/NetGene2/) indicated that this G → A substitution could potentially disrupt the splicing site between the second intron and the third exon.

Photosynthesis-Related Measurements

Wild-type (Col-0), *gox1-1*, and *gox2-1* lines were grown in soil under 60 to 100 μmol photons m^{-2} s^{-1} light intensity and a 12 h/12 h light/dark photoperiod. Following a dark adaptation period of 20 min, 3-week-old plants were transferred to an Imaging-PAM (M-series; Heinz Walz), and the minimal (F_o) and maximal (F_m) fluorescence was determined for the dark-adapted state. In one set of experiments, plants were exposed to blue light (700 μmol photons m^{-2} s^{-1}) for 10 h. The measuring beam was applied once every minute throughout the experiment to probe steady-state fluorescence under light (F_s). Saturating flashes were triggered every 10 min to assess maximal fluorescence under light (F_m'). The apparent ETR through PSII was calculated as follows: $ETR = 0.5 \times ([F_m' - F_s]/F_m') \times PAR \times 0.84$. NPQ was calculated as: $NPQ = (F_m - F_m')/F_m'$. In another set of experiments, plants were exposed to 15 consecutive 1-h periods of blue light (900 μmol m^{-2} s^{-1}) each followed by 23 min of darkness. Maximal quantum yield of PSII was calculated as $F_v/F_m = (F_m - F_o)/F_m$.

To probe the dephosphorylation state of the light-harvesting antennae of PSII (LHCBII), plants treated with continuous blue light (700 μmol photons m^{-2} s^{-1}) were harvested at 0, 45, 120, and 300 min from the onset of the light treatment. Total protein extracts were separated by SDS-PAGE and immunoblotted with an anti-phospho-Thr antibody (Cell Signaling).

Evolutionary Analysis

To obtain conserved synteny blocks containing *GOX1* and *GOX2*, we queried the synteny browser GenomicusPlants (v16.03; Louis et al., 2015) with *GOX1*. The synteny blocks were then visualized using the R package "genoPlotR" (Guy et al., 2010). To further confirm the loss of *GOX2* in *Arabidopsis lyrata*, we extracted the corresponding genomics sequence that, according to the conserved synteny block, is supposed to contain *GOX2*. We then predicted a gene model by aligning the protein sequence of *GOX2* from *Arabidopsis thaliana* with GeneWise (Birney et al., 2004). No gene showing similarity to *GOX2* was predicted in that genomic region.

We then reconstructed an amino acid-based phylogeny of the *GOX* genes present in the above identified conserved synteny blocks (Supplemental Table S6). To this end, we performed a multiple sequence alignment with T-Coffee and used trimAl 1.4 (Capella-Gutiérrez et al., 2009) to remove low-quality aligned regions in a heuristic approach (*automated1*). After the first round of multiple sequence alignment, a gene in *Brassica rapa* (Bra027339) exhibited large insertions in comparison to other sequences, indicating an annotation error. We hence used the protein sequence of *GOX1* from Arabidopsis to predict a gene model in the genomic sequence of Bra027339 by GeneWise and identified a gene with a similar length to the other *GOX* genes. After a new round of multiple sequence alignment with the predicted gene, we tested all available amino acid substitution matrices using ProtTest3 (Darriba et al., 2011) and selected the best-fit model according to Akaike Information Criterion (AIC), Bayesian Information Criterion (BIC) score and corrected AIC (AICc). The LG+GAMMA model outperformed the others and was used in PhyML 3.0 (Guindon et al., 2010) to search the maximum likelihood tree. PhyML made use of a neighbor-joining tree as the initial tree and optimized tree topology, branch lengths, and rate parameters. The best tree produced from either Nearest Neighbor Interchange or Subtree Pruning and Regrafting was retained as the maximum likelihood tree. Branch support values were obtained in a bootstrap analysis with 1,000 replicates. The "ggtree" package implemented in Bioconductor was used to visualize the obtained maximum likelihood tree.

To explore the evolutionary forces experienced from the *GOX1* and *GOX2* clades, we used "codeml" implemented in PAML (Yang, 2007). After back-translating amino acid alignment into nucleotide sequence alignment with trimAl 1.4, we compared a one-ratio model, in which all clades in the tree have the same ω value, with a three-ratio model, in which the *GOX1* and *GOX2* clades can have different ω values using the Solanaceae clade as a background. To further test whether the evolutionary pressures on the two postduplication branches were different after the duplication event but before the divergence of Brassicaceae, we performed a series of analyses with branch models and compared ω values on the two postduplication branches using the rest of the branches as a background (Supplemental Table S1). Then, a group of likelihood ratio tests was carried out to compare different models (Supplemental Table S2). To screen possible positive selections on sites along specific branches in Arabidopsis *GOX2*, we applied the modified branch-site model in PAML to each of the six branches leading to *GOX2* in Arabidopsis after the duplication event. The ω values in the modified branch model were allowed to vary across branches on the tree as well as among sites in the sequence (Zhang et al., 2005).

GC-MS Analysis

Metabolites were extracted from 50 mg fresh weight material ground under liquid nitrogen in 600 μL ice-cold *N,N*-dimethiylformamide in the presence of ribitol (30 μL from 0.2 mg/mL aqueous solution) used as an internal standard. After the addition of 400 μL water, the samples were shaken for 10 min at 4°C and subsequently centrifuged for 8 min at 14,000*g*. The aqueous phase was transferred to a new tube and vigorously mixed with 600 μL xylene for 10 min before centrifugation for 3 min at 14,000*g*. Aliquots (300 μL) from the lower

aqueous phase were dried under vacuum, and the residue was derivatized for 120 min at 37°C (in 40 μL of 20 mg mL^{-1} methoxyamine hydrochloride in pyridine) followed by a 30-min treatment at 37°C with 70 μL of MSTFA. The GC-MS system used was a gas chromatograph coupled to a time-of-flight mass spectrometer (Leco Pegasus HT TOF-MS). An autosampler Gerstel Multi Purpose system injected the samples. Helium was used as carrier gas at a constant flow rate of 2 mL s^{-1}, and gas chromatography was performed on a 30-m DB-35 column. The injection temperature was 230°C, and the transfer line and ion source were set to 250°C. The initial temperature of the oven (85°C) increased at a rate of 15°C/min up to a final temperature of 360°C. After a solvent delay of 180 s, mass spectra were recorded at 20 scans s^{-1} with *m/z* 70 to 600 scanning range. Chromatograms and mass spectra were evaluated by using Chroma TOF 4.5 (Leco) and TagFinder 4.2 software as described by Lisec et al. (2006).

RNA-Seq Analysis

cat2-2, *cat2-2 gox1-1*, and *cat2-2 gox2-1* mutant plants were grown under elevated CO_2 concentrations (3,000 μL L^{-1}) to impair photorespiration. Individual plants were organized according to a completely randomized block design in a controlled climate chamber (Votsch Industrietechnik) in a 16-h/8-h light/dark regime (relative humidity of 75%, 21°C, and an irradiance of 120 μmol m^{-2} s^{-1}). For high light treatments, 3-week-old plants were transferred to a Sanyo Fitotron growth chamber (Weiss Technik) in ambient air (~400 μL L^{-1} CO_2, relative humidity of 55%, 21°C) and irradiation of 1,000 μmol m^{-2} s^{-1} for 3 h. Middle aged leaves of 15 individual plants per line were sampled, pooled, and frozen in liquid nitrogen. This entire setup was repeated to obtain three biological repeats. Shoot tissue was sampled in three biological replicates before (t = 0) and after 3 h of treatment. RNA was extracted using a combination of TRIzol and RNeasy kit (Qiagen) according to the manufacturer's instructions. Library preparation and sequencing was performed at the VIB Nucleomics Core. Sequencing libraries were constructed with using the TruSeq Stranded mRNA Library Preparation Kit (Illumina). Three biological replicates were sequenced on Illumina NextSEquation 500, resulting in approximately 20 million 75-bp single-end reads per sample. Adapter sequences and low quality base pairs (Q < 20) were trimmed using Trim Galore (v0.3.3; http://www.bioinformatics.babraham.ac.uk/projects/trim_galore/), retaining high-quality reads of at least 50 bp length. Quality-filtered reads were aligned to the TAIR10 Arabidopsis reference genome using the spliced aligner TopHat2 (v2.1.0). The number of reads per gene was quantified using featureCounts function as implemented in the Subread package v1.4.6. Reads mapping to genes annotated as microRNA, pseudogenes, and protein coding genes (TAIR10) were retained for further downstream analysis (28,517 genes in total).

Differentially expressed genes were identified using the R (v3.1.2) software package edgeR. For the analysis genes with expression values higher than 0.21 cpm (corresponding to five read counts) in at least three samples were retained (19,719 genes). TMM normalization was applied using the "calcNormFactors" function. Variability in the data set was assessed with a MDSplot employing the 3,000 top genes to calculate pairwise distances (top = 3000). There was a clear separation according to photorespiratory treatment; however, the third replicate also showed separation, especially under control conditions. Trended negative binomial dispersion parameters were estimated based on a model with main effects of genotype, treatment, replicate, and an interaction term between genotype and treatment using the "estimateGLMTrendedDisp" function, followed by the estimation of the empirical Bayes dispersion for each transcript. A negative binomial regression model was then used to model the overdispersed counts for each gene separately with fixed values for the dispersion parameter as implemented in the function glmFit using the above described model. A likelihood ratio test was performed to compare this model with a model without replicate to assess possible replicate (batch) effects. After FDR adjustments of the *P* values with the Benjamini and Hochberg method, 4,931 genes were found to have a significant batch effect as was expected by the MDS plot. Hence, we omitted the third replicate and used solely the first and second replicates for which 19,712 genes had expression values higher than 0.21 cpm (corresponding to five read counts) in at least two samples. The MDS plot showed a more pronounced effect in the absence of GOX1 under stress than the previous one including all three replicates. Following the same procedure as described above, a neglectable batch effect was observed. The estimate of the dispersions and the fitting of the model was repeated with only the main effects of stress treatment and genotype (*cat2-2 gox1-1* and *cat2-2 gox2-1*) and treatment and their interaction. A likelihood ratio test followed by FDR adjustment showed 608 genes and 1 gene to be affected (FDR < 0.05) under stress due the lack of GOX1 or GOX2, respectively, which was in line with the MDS plot. To test user-defined hypotheses, a no intercept single-factor model was defined combining genotype and treatment factors (e.g. *cat2-2_3h*). Dispersions were estimated using the "estimateGLMRobustDisp" function. A negative binomial regression model was then used to model the overdispersed counts for each gene separately with fixed values for the dispersion parameter as outlined in McCarthy et al. (2012) and as implemented in the function "glmFit" using the above described model. Hypothesis testing was based on likelihood ratio tests. Contrasts of interest were the response between different genotypes under control conditions (t = 0 h) and the effect of photorespiratory stress in each genotype.

Identification of ROS-Responsive Genes

In order to generate a robust ROS signature the raw intensity (.CEL), files from five studies featuring ROS-generating conditions were obtained from the Gene Expression Omnibus (http://www.ncbi.nlm.nih.gov/geo/) and ArrayExpress (http://www.ebi.ac.uk/arrayexpress/). The following experiments were considered: reillumination of the conditional *flu* mutant for 2 h following a dark acclimation (GSE10812); treatment of seedlings with oligomycin for 4 h (GSE38965); treatment of seedlings with 50 μM antimycin A for 3 h (GSE41136); exposure of seedlings to ozone for 6 h (E-MEXP-342); treatment of seedlings with 10 mM H_2O_2 for 24 h. All raw intensity files were normalized by robust multiarray averaging using the Bioconductor package affy (v1.40.0). Probe sets were up to date using the TAIR10 CDF annotation retrieved from BrainArray (TAIRG v18.0.0; http://brainarray.mbni.med.umich.edu/). Differential gene expression was analyzed with the limma package (v3.18.13) using empirical Bayes moderated t-statistics. Differentially expressed genes were selected for each transcriptomic response, using a *P* value of 0.01 as a significance threshold and absolute $\log_2$ fold change greater than 1. Differential gene expression values were imported into the TM4 Microarray Software suite Multi Experiment Viewer v4.9.0 (TIGR). Genes were hierarchically clustered using Euclidean distance with average linkage.

Quantitative RT-PCR

For quantification of expression levels, total RNA was extracted from 3-week-old rosettes with the RNeasy Plant Mini Kit (Qiagen). First-strand cDNA synthesis was performed with iScript cDNA Synthesis Kit with 1 μg of total RNA used as input material. Five microliters of the 1:8 diluted first-strand cDNA was used as a template in subsequent PCR performed on the iCycler iQ (Bio-Rad) with respective gene specific primers (Supplemental Table S3). Reactions were performed in three technical repeats with the SYBR Green I Master Kit according to the manufacturer's instructions. Expression analysis was performed with qBASEPlus software (Biogazelle) with *ELONGATION FACTOR1α* (*EF-1α*) and *POLYUBIQUTIN5* (*UBIQ5*) used for data normalization.

All experiments were performed with four biological replicates. Statistical analysis was carried out with one-way ANOVA followed by the Tukey-Kramer post-hoc test.

GOX Enzyme Assays

The glycolate oxidase activity was measured using the *o*-Dianisidine method described before (Rojas et al., 2012) downscaled for 200 mg ground tissue. The shoot tissue was collected and frozen in liquid nitrogen and ground with ball mill (Retsch). The material was then mixed with 1 mL of extraction buffer by vortexing and centrifuged at 16,100*g* for 30 min at 4°C. The protein concentration in soluble phase was determined with Bradford Assay (Bradford, 1976). Next, 10 μL supernatant was used in spectrophotometric glycolate oxidase activity assay conducted in VersaMax microplate reader (Molecular Devices) at room temperature for 1 h. Specific activity was calculated by dividing ΔA by time and amount of protein present in the sample and expressed as percentage of control. All enzymatic assays were performed on three biological replicates with three technical repeats.

Alternatively, GOX activity was assessed as described by Yamaguchi and Nishimura (2000) with minor modifications. Briefly, 100 mg plant material ground under liquid nitrogen was homogenized in 100 mM HEPES (pH 7.2) containing 1 mM EDTA and 10 mM 2-mercaptoethanol. Following centrifugation, 10 μL supernatant was introduced in 180 μL reaction medium (100 mM triethanolamine, pH 7.8, 3 mM EDTA, 0.75 mM oxidized glutathione, and 4 mM phenylhydrazine), and the reaction was started with 2.3 mM glycolate. The amount of enzyme catalyzing the production of 1 μmol glyoxylate-phenylhydrazone

min^{-1} based on the extinction coefficient for phenylhydrazone at 324 nm ($16.8\ mM^{-1}\ cm^{-1}$) was defined as one unit. The enzyme activity was expressed as mU per mg protein determined as described above.

Accession Numbers

Sequence data from this article can be found in the GenBank/EMBL data libraries under accession numbers GSE77170 and GSE77171.

Supplemental Data

The following supplemental materials are available.

Supplemental Figure S1. *GOX1* and *GOX2* gene models.

Supplemental Figure S2. Read coverage of *GOX1* and *GOX2* loci from RNA-seq analysis of *cat2-2 gox1-1*, *cat2-2*, and *cat2-2 gox2-1* mutants.

Supplemental Figure S3. Heat map of differentially expressed transcripts ($|\log_2 FC| > 1$, FDR < 0.05) between *cat2-2 gox1-1*, *cat2-2 gox2-1*, and *cat2-2* mutants under control high CO_2 conditions aimed at inhibiting the photorespiratory flux.

Supplemental Figure S4. Redox status of Col-0, *cat2-2*, *cat2-2 gox1-1*, and *cat2-2 gox2-1* plants grown under ambient air and moderate light intensity (300 μmol m^{-2} s^{-1}).

Supplemental Figure S5. Nonphotochemical quenching and phosphorylation of LHCBII upon exposure of Col-0, *gox1-1*, and *gox2-1* plants grown under conditions limiting photorespiration to high light.

Supplemental Figure S6. *GOX1* and *GOX2* genes in Brassicaceae are clustered as monophyly in the gene tree of ORTHO03D000507 from PLAZA 3.0 dicots.

Supplemental Figure S7. Extractable leaf GOX activity.

Supplemental Figure S8. *GOX1* and *GOX2* transcript abundance.

Supplemental Table S1. Maximum likelihood estimates of parameters under branch models on both postduplication branches leading to the *GOX1* and *GOX2* clades.

Supplemental Table S2. Likelihood ratio tests for comparing different branch models applied to both postduplication branches leading to the *GOX1* and *GOX2* clades.

Supplemental Table S3. The modified branch-site models for detecting positive selection on six branches after the duplication event leading to *GOX2* in Arabidopsis.

Supplemental Table S4. List of primers used in this study.

Supplemental Table S5. Mutations enriched in line *238.3*.

Supplemental Table S6. Data sources and sequence accessions.

Supplemental Data Set 1. RNA-seq results.

Supplemental Data Set 2. List of transcripts that responded to the photorespiratory stress treatment in a genotype-specific manner.

Supplemental Data Set 3. Gene Set Enrichment Analysis (http://structuralbiology.cau.edu.cn/PlantGSEA) of the transcripts that responded to the photorespiratory stress treatment in a genotype-specific manner.

Received March 3, 2016; accepted May 23, 2016; published May 25, 2016.

LITERATURE CITED

Abat JK, Mattoo AK, Deswal R (2008) S-nitrosylated proteins of a medicinal CAM plant *Kalanchoe pinnata*- ribulose-1,5-bisphosphate carboxylase/oxygenase activity targeted for inhibition. FEBS J **275:** 2862–2872

Bailey CD, Koch MA, Mayer M, Mummenhoff K, O'Kane SL, Jr., Warwick SI, Windham MD, Al-Shehbaz IA (2006) Toward a global phylogeny of the *Brassicaceae*. Mol Biol Evol **23:** 2142–2160

Bauwe H, Hagemann M, Kern R, Timm S (2012) Photorespiration has a dual origin and manifold links to central metabolism. Curr Opin Plant Biol **15:** 269–275

Birney E, Clamp M, Durbin R (2004) GeneWise and Genomewise. Genome Res **14:** 988–995

Bradford MM (1976) A rapid and sensitive method for the quantitation of microgram quantities of protein utilizing the principle of protein-dye binding. Anal Biochem **72:** 248–254

Capella-Gutiérrez S, Silla-Martínez JM, Gabaldón T (2009) trimAl: a tool for automated alignment trimming in large-scale phylogenetic analyses. Bioinformatics **25:** 1972–1973

Caverzan A, Passaia G, Rosa SB, Ribeiro CW, Lazzarotto F, Margis-Pinheiro M (2012) Plant responses to stresses: Role of ascorbate peroxidase in the antioxidant protection. Genet Mol Biol **35:** 1011–1019

Darriba D, Taboada GL, Doallo R, Posada D (2011) ProtTest 3: fast selection of best-fit models of protein evolution. Bioinformatics **27:** 1164–1165

Davletova S, Rizhsky L, Liang H, Shengqiang Z, Oliver DJ, Coutu J, Shulaev V, Schlauch K, Mittler R (2005) Cytosolic ascorbate peroxidase 1 is a central component of the reactive oxygen gene network of Arabidopsis. Plant Cell **17:** 268–281

Dellero Y, Jossier M, Glab N, Oury C, Tcherkez G, Hodges M (2016) Decreased glycolate oxidase activity leads to altered carbon allocation and leaf senescence after a transfer from high CO_2 to ambient air in *Arabidopsis thaliana*. J Exp Bot **67:** 3149–3163

Dellero Y, Mauve C, Boex-Fontvieille E, Flesch V, Jossier M, Tcherkez G, Hodges M (2015) Experimental evidence for a hydride transfer mechanism in plant glycolate oxidase catalysis. J Biol Chem **290:** 1689–1698

Dietz KJ (2016) Thiol-based peroxidases and ascorbate peroxidases: why plants rely on multiple peroxidase systems in the photosynthesizing chloroplast? Mol Cells **39:** 20–25

Engqvist MKM, Schmitz J, Gertzmann A, Florian A, Jaspert N, Arif M, Balazadeh S, Mueller-Roeber B, Fernie AR, Maurino VG (2015) GLYCOLATE OXIDASE3, a glycolate oxidase homolog of yeast l-lactate Cytochrome c Oxidoreductase, supports l-lactate oxidation in roots of *Arabidopsis*. Plant Physiol **169:** 1042–1061

Esser C, Kuhn A, Groth G, Lercher MJ, Maurino VG (2014) Plant and animal glycolate oxidases have a common eukaryotic ancestor and convergently duplicated to evolve long-chain 2-hydroxy acid oxidases. Mol Biol Evol **31:** 1089–1101

Foyer CH, Bloom AJ, Queval G, Noctor G (2009) Photorespiratory metabolism: genes, mutants, energetics, and redox signaling. Annu Rev Plant Biol **60:** 455–484

Guindon S, Dufayard JF, Lefort V, Anisimova M, Hordijk W, Gascuel O (2010) New algorithms and methods to estimate maximum-likelihood phylogenies: assessing the performance of PhyML 3.0. Syst Biol **59:** 307–321

Guy L, Kultima JR, Andersson SG (2010) genoPlotR: comparative gene and genome visualization in R. Bioinformatics **26:** 2334–2335

Hartwig B, James GV, Konrad K, Schneeberger K, Turck F (2012) Fast isogenic mapping-by-sequencing of ethyl methanesulfonate-induced mutant bulks. Plant Physiol **160:** 591–600

Hodges M, Dellero Y, Keech O, Betti M, Raghavendra AS, Sage R, Zhu XG, Allen DK, Weber AP (2016) Perspectives for a better understanding of the metabolic integration of photorespiration within a complex plant primary metabolism network. J Exp Bot **67:** 3015–3026

Hodges M, Jossier M, Boex-Fontvieille E, Tcherkez G (2013) Protein phosphorylation and photorespiration. Plant Biol (Stuttg) **15:** 694–706

Kaurilind E, Xu E, Brosché M (2015) A genetic framework for H_2O_2 induced cell death in *Arabidopsis thaliana*. BMC Genomics **16:** 837

Kerchev P, Mühlenbock P, Denecker J, Morreel K, Hoeberichts FA, Van Der Kelen K, Vandorpe M, Nguyen L, Audenaert D, Van Breusegem F (2015) Activation of auxin signalling counteracts photorespiratory H_2O_2-dependent cell death. Plant Cell Environ **38:** 253–265

Lisec J, Schauer N, Kopka J, Willmitzer L, Fernie AR (2006) Gas chromatography mass spectrometry-based metabolite profiling in plants. Nat Protoc **1:** 387–396

Lobell DB, Gourdji SM (2012) The influence of climate change on global crop productivity. Plant Physiol **160:** 1686–1697

Louis A, Murat F, Salse J, Crollius HR (2015) GenomicusPlants: a web resource to study genome evolution in flowering plants. Plant Cell Physiol **56:** e4

Maruta T, Tanouchi A, Tamoi M, Yabuta Y, Yoshimura K, Ishikawa T, Shigeoka S (2010) Arabidopsis chloroplastic ascorbate peroxidase isoenzymes play a dual role in photoprotection and gene regulation under photooxidative stress. Plant Cell Physiol **51:** 190–200

Massey V (1994) Activation of molecular oxygen by flavins and flavoproteins. J Biol Chem **269:** 22459–22462

McCarthy DJ, Chen Y, Smyth GK (2012) Differential expression analysis of multifactor RNA-Seq experiments with respect to biological variation. Nucleic Acids Res **40:** 4288–4297

Mittler R, Vanderauwera S, Gollery M, Van Breusegem F (2004) Reactive oxygen gene network of plants. Trends Plant Sci **9:** 490–498

Narendra S, Venkataramani S, Shen G, Wang J, Pasapula V, Lin Y, Kornyeyev D, Holaday AS, Zhang H (2006) The Arabidopsis ascorbate peroxidase 3 is a peroxisomal membrane-bound antioxidant enzyme and is dispensable for Arabidopsis growth and development. J Exp Bot **57:** 3033–3042

Noctor G, Veljovic-Jovanovic S, Driscoll S, Novitskaya L, Foyer CH (2002) Drought and oxidative load in the leaves of C3 plants: a predominant role for photorespiration? Ann Bot **89:** 841–850

Ortega-Galisteo AP, Rodríguez-Serrano M, Pazmiño DM, Gupta DK, Sandalio LM, Romero-Puertas MC (2012) S-Nitrosylated proteins in pea (*Pisum sativum* L.) leaf peroxisomes: changes under abiotic stress. J Exp Bot **63:** 2089–2103

Pick TR, Bräutigam A, Schulz MA, Obata T, Fernie AR, Weber APM (2013) PLGG1, a plastidic glycolate glycerate transporter, is required for photorespiration and defines a unique class of metabolite transporters. Proc Natl Acad Sci USA **110:** 3185–3190

Proost S, Van Bel M, Vaneechoutte D, Van de Peer Y, Inzé D, Mueller-Roeber B, Vandepoele K (2015) PLAZA 3.0: an access point for plant comparative genomics. Nucleic Acids Res **43:** D974–D981

Pnueli L, Liang H, Rozenberg M, Mittler R (2003) Growth suppression, altered stomatal responses, and augmented induction of heat shock proteins in cytosolic ascorbate peroxidase (Apx1)-deficient Arabidopsis plants. Plant J **34:** 187–203

Queval G, Issakidis-Bourguet E, Hoeberichts FA, Vandorpe M, Gakière B, Vanacker H, Miginiac-Maslow M, Van Breusegem F, Noctor G (2007) Conditional oxidative stress responses in the *Arabidopsis* photorespiratory mutant *cat2* demonstrate that redox state is a key modulator of daylength-dependent gene expression, and define photoperiod as a crucial factor in the regulation of H_2O_2-induced cell death. Plant J **52:** 640–657

Reumann S, Babujee L, Ma C, Wienkoop S, Siemsen T, Antonicelli GE, Rasche N, Lüder F, Weckwerth W, Jahn O (2007) Proteome analysis of *Arabidopsis* leaf peroxisomes reveals novel targeting peptides, metabolic pathways, and defense mechanisms. Plant Cell **19:** 3170–3193

Rochaix JD (2014) Regulation and dynamics of the light-harvesting system. Annu Rev Plant Biol **65:** 287–309

Rojas CM, Senthil-Kumar M, Wang K, Ryu C-M, Kaundal A, Mysore KS (2012) Glycolate oxidase modulates reactive oxygen species-mediated signal transduction during nonhost resistance in *Nicotiana benthamiana* and *Arabidopsis*. Plant Cell **24:** 336–352

Rouhier N, Villarejo A, Srivastava M, Gelhaye E, Keech O, Droux M, Finkemeier I, Samuelsson G, Dietz KJ, Jacquot JP, Wingsle G (2005) Identification of plant glutaredoxin targets. Antioxid Redox Signal **7:** 919–929

Sage RF, Christin PA, Edwards EJ (2011) The C(4) plant lineages of planet Earth. J Exp Bot **62:** 3155–3169

Schäfer L, Feierabend J (2000) Photoinactivation and protection of glycolate oxidase *in vitro* and in leaves. Z Naturforsch C **55:** 361–372

Schneeberger K, Ossowski S, Lanz C, Juul T, Petersen AH, Nielsen KL, Jørgensen J-E, Weigel D, Andersen SU (2009) SHOREmap: simultaneous mapping and mutation identification by deep sequencing. Nat Methods **6:** 550–551

Timm S, Bauwe H (2013) The variety of photorespiratory phenotypes - employing the current status for future research directions on photorespiration. Plant Biol (Stuttg) **15:** 737–747

Timm S, Florian A, Jahnke K, Nunes-Nesi A, Fernie AR, Bauwe H (2011) The hydroxypyruvate-reducing system in *Arabidopsis*: multiple enzymes for the same end. Plant Physiol **155:** 694–705

Timm S, Nunes-Nesi A, Pärnik T, Morgenthal K, Wienkoop S, Keerberg O, Weckwerth W, Kleczkowski LA, Fernie AR, Bauwe H (2008) A cytosolic pathway for the conversion of hydroxypyruvate to glycerate during photorespiration in *Arabidopsis*. Plant Cell **20:** 2848–2859

Vanderauwera S, Suzuki N, Miller G, van de Cotte B, Morsa S, Ravanat J-L, Hegie A, Triantaphylidès C, Shulaev V, Van Montagu MCE, Van Breusegem F, Mittler R (2011) Extranuclear protection of chromosomal DNA from oxidative stress. Proc Natl Acad Sci USA **108:** 1711–1716

Walker BJ, VanLoocke A, Bernacchi CJ, Ort DR (2016) The costs of photorespiration to food production now and in the future. Annu Rev Plant Biol **67:** 107–129

Wang X, Wang H, Wang J, Sun R, Wu J, Liu S, Bai Y, Mun JH, Bancroft I, Cheng F, et al; Brassica rapa Genome Sequencing Project Consortium (2011) The genome of the mesopolyploid crop species Brassica rapa. Nat Genet **43:** 1035–1039

Waszczak C, Kerchev K, Mühlenbock P, Frank A. Hoeberichts, Van Der Kelen K, Mhamdi A, Willems P, Denecker J, Kumpf R, Noctor G, Messens J, Van Breusegem F (2016) SHORT-ROOT deficiency alleviates the cell death phenotype of the Arabidopsis *catalase2* mutant under photorespiration-promoting conditions. Plant Cell, in press

Wheeler T, von Braun J (2013) Climate change impacts on global food security. Science **341:** 508–513

Willems P, Mhamdi A, Stael S, Storme V, Kerchev PI, Noctor G, Gevaert K, Van Breusegem F (2016) The ROS Wheel: refining ROS transcriptional footprints in Arabidopsis. Plant Physiol **171:** 1720–1733

Xu H, Zhang J, Zeng J, Jiang L, Liu E, Peng C, He Z, Peng X (2009) Inducible antisense suppression of glycolate oxidase reveals its strong regulation over photosynthesis in rice. J Exp Bot **60:** 1799–1809

Yamaguchi K, Nishimura M (2000) Reduction to below threshold levels of glycolate oxidase activities in transgenic tobacco enhances photoinhibition during irradiation. Plant Cell Physiol **41:** 1397–1406

Yang Z (2007) PAML 4: phylogenetic analysis by maximum likelihood. Mol Biol Evol **24:** 1586–1591

Zhang J, Nielsen R, Yang Z (2005) Evaluation of an improved branch-site likelihood method for detecting positive selection at the molecular level. Mol Biol Evol **22:** 2472–2479

Zelitch I, Schultes NP, Peterson RB, Brown P, Brutnell TP (2009) High glycolate oxidase activity is required for survival of maize in normal air. Plant Physiol **149:** 195–204

Supplemental Figure S1.

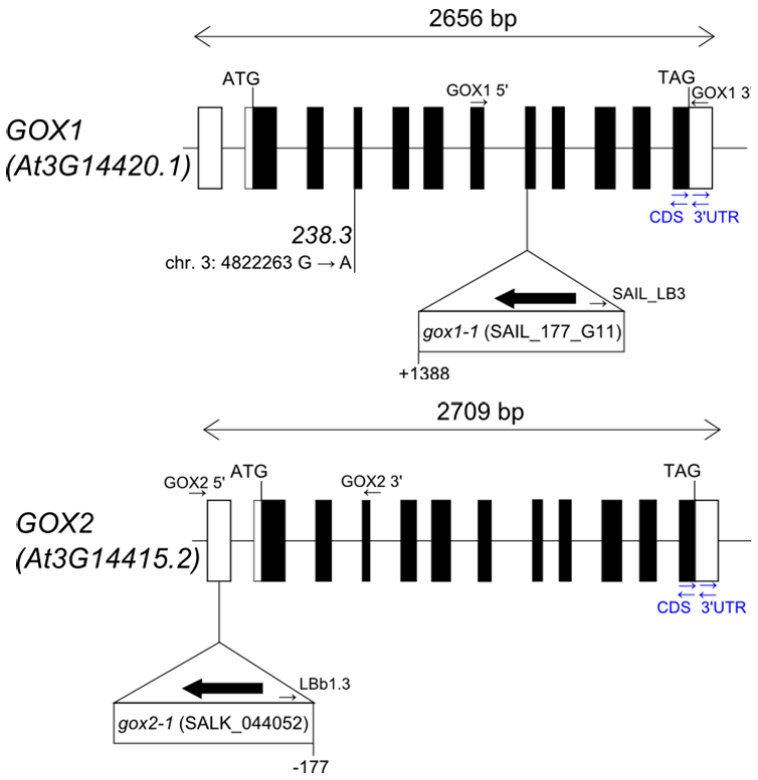

Supplemental Figure S1. *GOX1* and *GOX2* gene models, together with T-DNA insertion sites in the knockout SAIL_177_G11 (*gox1-1*) and SALK_044052 (*gox2-1*) lines, as well as the EMS-induced single nucleotide polymorphism in line *238.3*. Black and white boxes represent protein-coding and untranslated regions, respectively. Black arrows indicate primers used for genotyping and blue arrows – primers used for qRT-PCR.

Supplemental Figure S2.

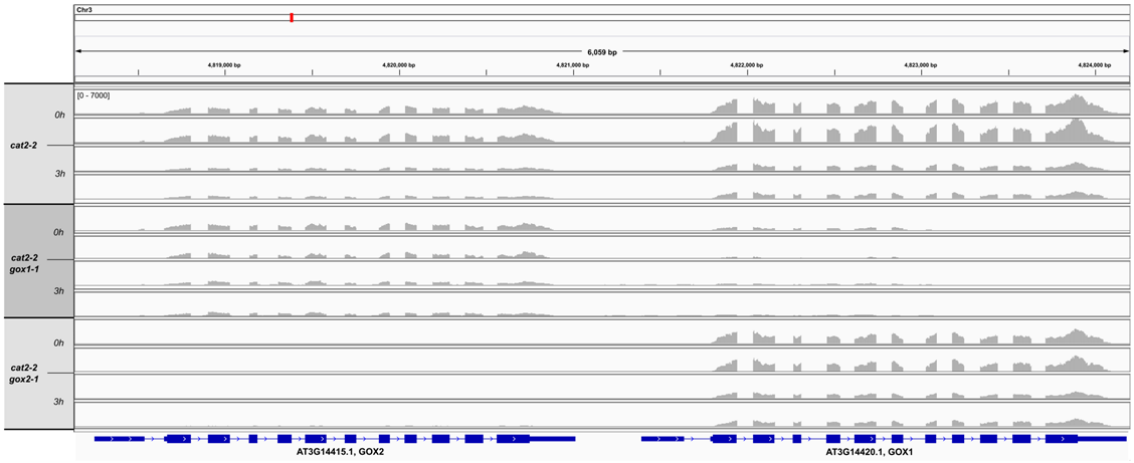

Supplemental Figure S2. Read coverage of *GOX1* and *GOX2* loci from RNA-seq analysis of *cat2-2 gox1-1*, *cat2-2* and *cat2-2 gox2-1* mutants. Aligning of reads obtained by RNA-seq from *cat2-2*, *cat2-2 gox1-1* and *cat2-2 gox2-2* mutants before (0h) and after exposure to photorespiratory stress (3h) to the reference sequences of *GOX1* and *GOX2*.

Supplemental Figure S3.

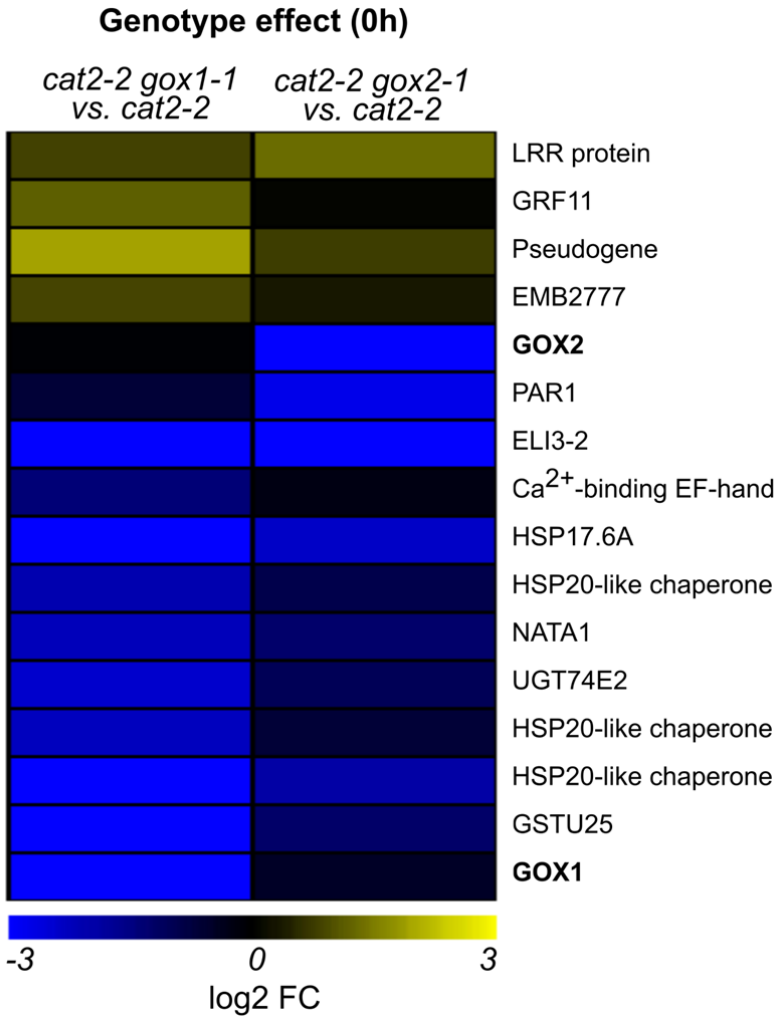

Supplemental Figure S3. Heat map of differentially expressed transcripts (|log2 FC| > 1, FDR < 0.05) between *cat2-2 gox1-1*, *cat2-2 gox2-1* and *cat2-2* mutants under control high CO_2 conditions aimed at inhibiting the photorespiratory flux.

Supplemental Figure S4.

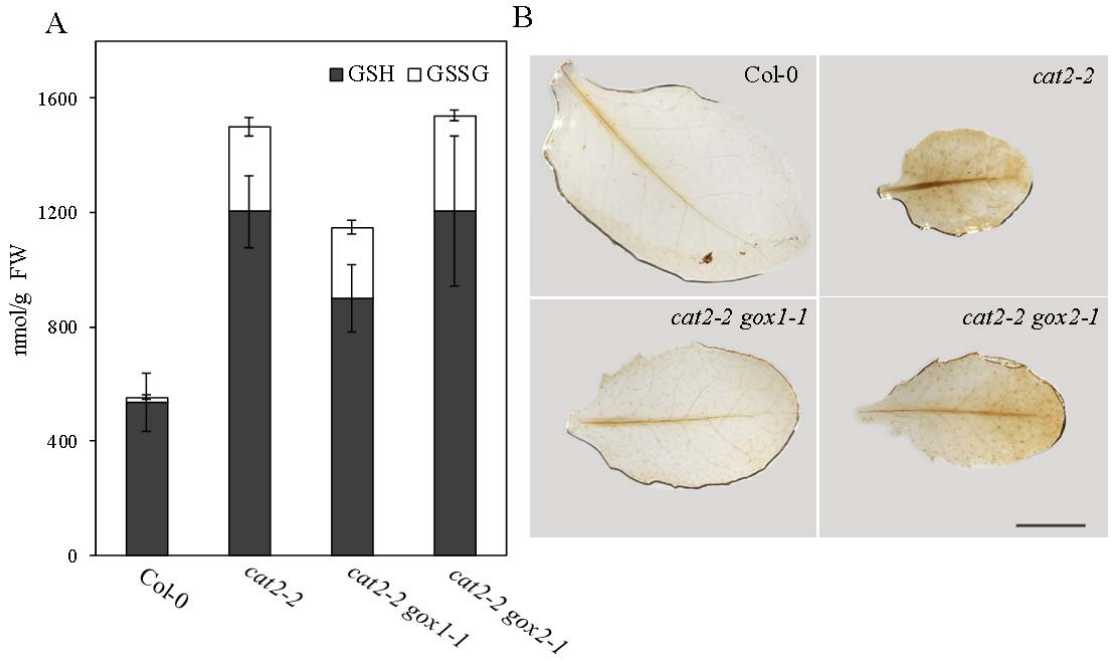

Supplemental Figure S4. Redox status of Col-0, *cat2-2*, *cat2-2 gox1-1* and *cat2-2 gox2-1* plants grown under ambient air and moderate light intensity (300 µmol m^{-2} s^{-1}). A) Levels of reduced and oxidized glutathione (GSH and GSSG, respectively) in rosettes of three-week-old plants. Bars represent means of three biological replicates ± SE. (B) Representative bright-field images of 3,3′-diaminobenzidine-stained mature leaves of three-week-old plants. The scale bar is 0,5 cm.

Supplemental Figure S5.

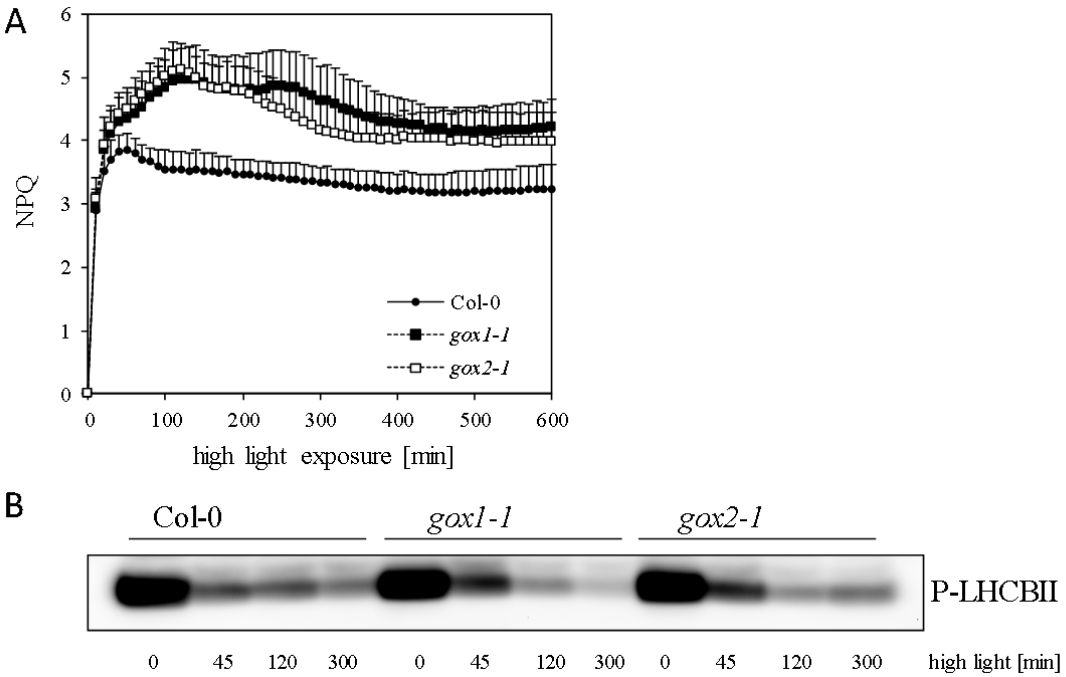

Supplemental Figure S5. Non-photochemical quenching (NPQ; A) and phosphorylation of LHCBII (B) upon exposure of Col-0, *gox1-1* and *gox2-1* plants grown under conditions limiting photorespiration to high light.

Supplemental Figure S6.

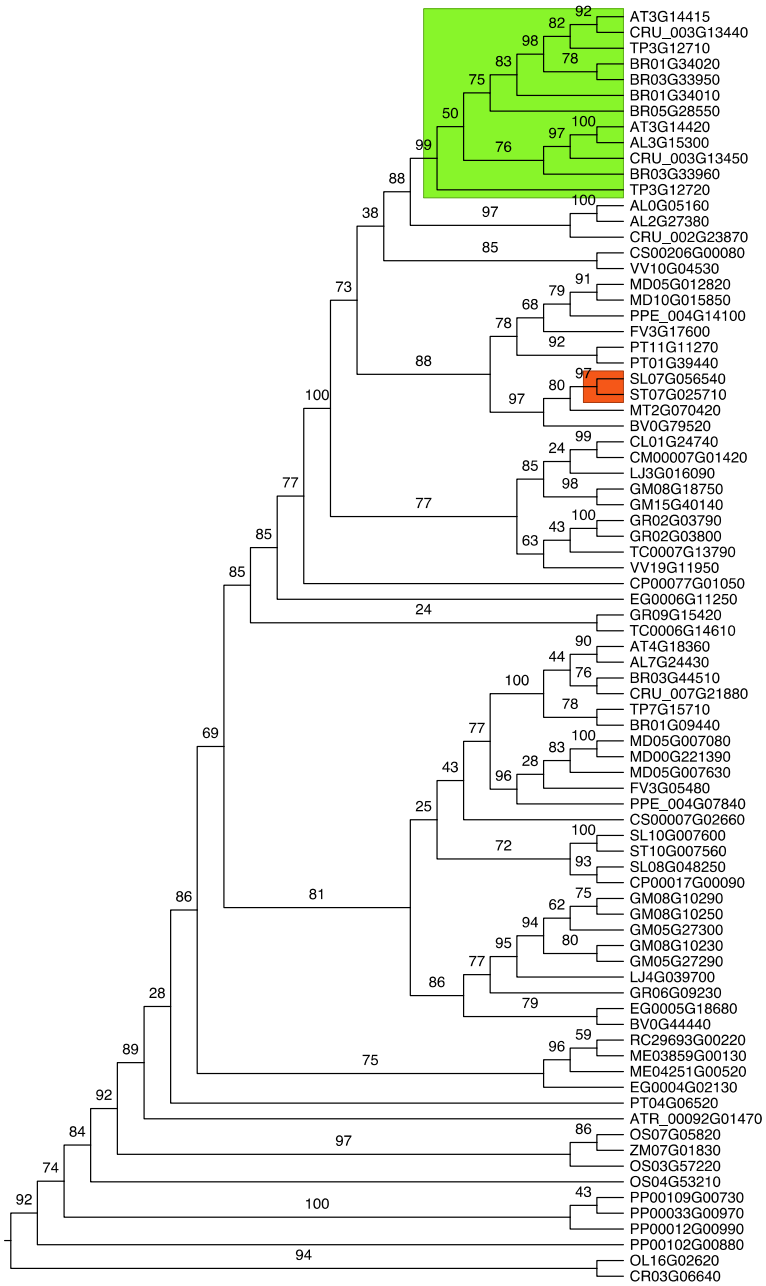

Supplemental Figure S6. *GOX1* and *GOX2* genes in *Brassicaceae* are clustered as monophyletic group in the gene tree of ORTHO03D000507 from PLAZA 3.0 Dicots. *GOX1* and *GOX2* in *Brassicaceae* are in green, and the two *GOX* genes from *Solanaceae* identified based on synteny are shown in red. Numbers on branches denote bootstrap values.

Supplemental Figure S7.

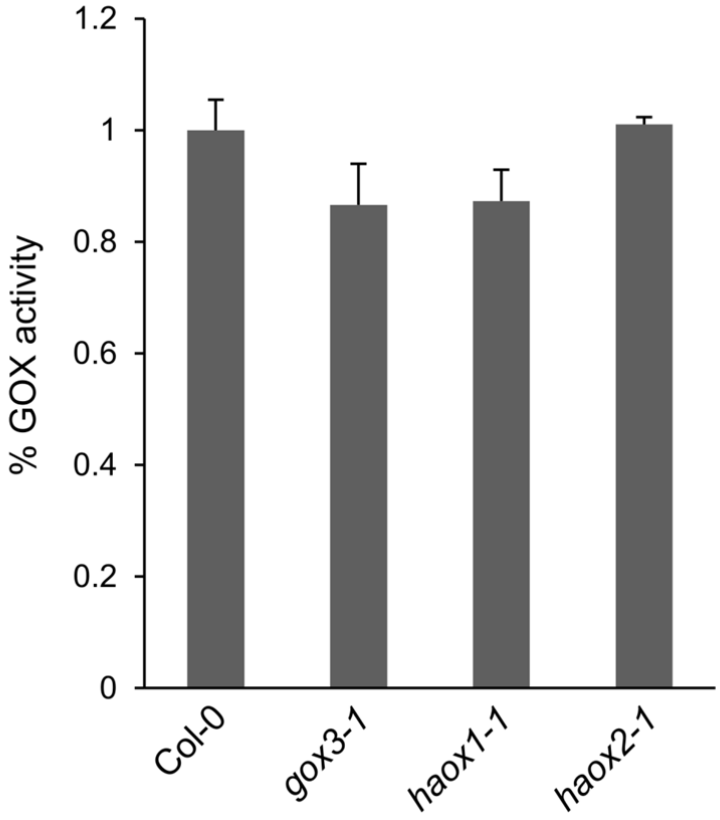

Supplemental Figure S7. Extractable leaf GOX activity. Bars represent averages from three biological replicates ± SE.

Supplemental Figure S8.

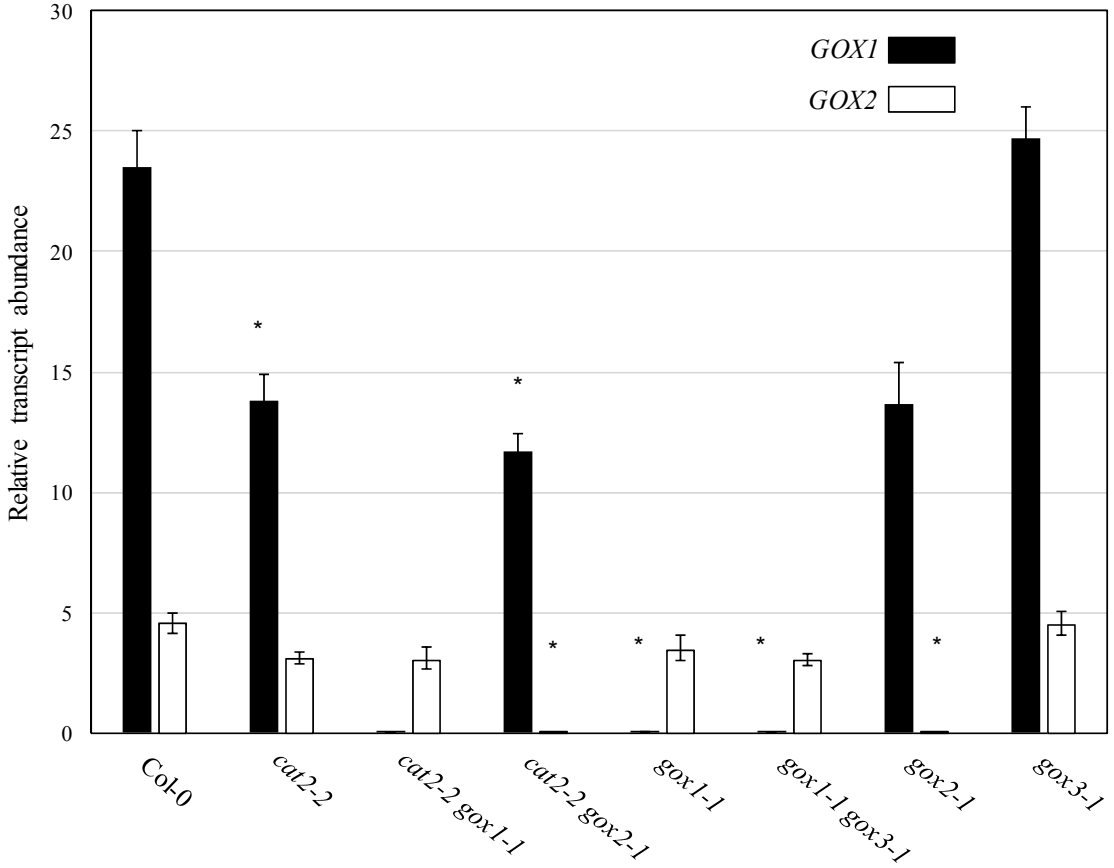

Supplemental Figure S8. *GOX1* and *GOX2* transcript abundance. RNA was extracted from rosettes of three-week-old plants grown *in vitro* and used to quantify gene expression levels by qRT-PCR. Values are means ± SD of four biological replicates. Asterisks indicate significant difference ($p<0.05$) in comparison to Col-0 according to one-way ANOVA.

Supplemental Table S1. Maximum likelihood estimates of parameters under branch models on both post-duplication branches leading to the *GOX1* and *GOX2* clades.

Model	p	ℓ	**κ**	ω_0	ω_{GOX1}	ω_{GOX2}
A: One ratio: $\omega_0 = \omega_{GOX1} = \omega_{GOX2}$	33	-5437.64	1.71	0.070	0.070	0.070
B: Two ratios: $\omega_0 = \omega_{GOX1}, \omega_{GOX2}$	34	-5432.37	1.69	0.067	0.067	31.293
C: Two ratios: $\omega_0 = \omega_{GOX2}, \omega_{GOX1}$	34	-5436.67	1.71	0.069	0.233	0.069
D: Two ratios: $\omega_0, \omega_{GOX1} = \omega_{GOX2}$	34	-5433.50	1.71	0.067	0.291	0.291
E: Three ratios: $\omega_0, \omega_{GOX1}, \omega_{GOX2}$	35	-5432.21	1.70	0.066	0.105	3.941
F: Two ratios: $\omega_0 = \omega_{GOX1}, \omega_{GOX2} = 1$	33	-5432.55	1.70	0.067	0.067	1.000
G: Two ratios: $\omega_0 = \omega_{GOX2}, \omega_{GOX1} = 1$	33	-5437.34	1.72	0.068	1.000	0.068
H: Two ratios: $\omega_0, \omega_{GOX1} = \omega_{GOX2} = 1$	33	-5436.17	1.72	0.066	1.000	1.000
I: Three ratios: $\omega_0, \omega_{GOX1}, \omega_{GOX2} = 1$	34	-5432.30	1.70	0.067	0.116	1.000
J: Three ratios: $\omega_0, \omega_{GOX2}, \omega_{GOX1} = 1$	34	-5435.07	1.73	0.066	1.000	0.275

p, number of free parameters in the model; ℓ, log-likelihood; **κ**, the ratio of transition to transversion; ω_{GOX1} and ω_{GOX2}, the ratio of non-synonymous substituion rate (dN) to synonymous substituion rate (dS) on the two post-duplication branches to *GOX1* and *GOX2* clades, respectively; ω_0, dN/dS for rest of the branches on the tree

Supplemental Table S2. Likelihood ratio tests for comparing different branch models applied to both post-duplication branches leading to the *GOX1* and *GOX2* clades.

Model comparisons	2$\Delta\ell$	df	*p* value
A-D	8.295754	1	0.003973788
A-B	10.542752	1	0.001166446
C-E	8.923886	1	0.00281465
A-C	1.944748	1	0.16315393
B-E	0.325882	1	0.568094036
D-H	5.342664	1	0.020809648
B-F	0.348118	1	0.555180423
E-I	0.177828	1	0.673246506
C-G	1.331848	1	0.248476723
E-J	5.729078	1	0.016686241

2$\Delta\ell$, likelyhood ratio statistics; df, degree of freedom

Supplemental Table S3. The modified branch-site models for detecting positive selection on six branches after the duplication event leading to *GOX2* in *Arabidopsis*.

Branch	ℓ_{H0}	ℓ_{HA}	$2\Delta\ell$	df	*p* value
#1	-5401.887282	-5401.781842	0.21088	1	0.32303927
#2	-5401.767414	-5401.577101	0.38062	1	0.26863420
#3	-5402.937338	-5402.85316	0.16835	1	0.34078851
#4	-5403.195792	-5403.195793	2E-06	1	0.49943581
#5	-5403.170388	-5403.170388	0	1	0.5
#6	-5402.919624	-5402.047157	1.74493	1	0.09325743

ℓ_{H0}, log likelihood for the branch-site model without positive selection; ℓ_{HA}, log likelihood for the branch-site model with positive selection; $2\Delta\ell$, likelyhood ratio statistics; df, degree of freedom

Supplemental Table S4. List of primers used in the study.

Primer name	Use	Sequence
gox1_SAIL_177_G11_newLP1	Genotyping	GGGAATCACAAGAAATTGATC
gox1_SAIL_177_G11_RP	Genotyping	GAAGGACTTGACCTCGGAAAG
gox2_SALK_044052_LP	Genotyping	ATACCATGATGGTTCCAGCAG
gox2_SALK_044052_RP	Genotyping	TTGTTATGTTTCGTCAAGCCC
gox3_GABI_523D09_LP	Genotyping	TTGGATGGGAATACTTTATTGG
gox3_GABI_523D09_RP	Genotyping	GCATCAACCTTTTGCTTGAAG
haox1_SAIL_84_A04_newLP2	Genotyping	AGAGGACAAGAGGAGCAAGATTC
haox1_SAIL_84_A04_RP	Genotyping	GCGCTTTGAAAACATCTGTTC
haox2_SALK_102409_LP	Genotyping	GGAAACTTGGTCTCCATCAGG
haox2_SALK_102409_RP	Genotyping	GCTCGACTATTCCCCTGCTAC
LBb1.3	Genotyping	ATTTTGCCGATTTCGGAAC
SAIL_LB3	Genotyping	TAGCATCTGAATTTCATAACCAATCTCGATACAC
GK_o8474	Genotyping	ATAATAACGCTGCGGACATCTACATTTT
SALK_newLB1	Genotyping	TGGACCGCTTGCTGCAACTCTC
CAT2_LP	Genotyping	CCCAGAGGTACCTCTTCTTCTCCCATG
CAT2_RP	Genotyping	TCAGGGAACTTCATCCCATCGC
GOX1_F_CDS	qRT-PCR	TCTCATTGGCAGCTGAAGGA
GOX1_R_CDS	qRT-PCR	GAGTGTCCCATTCGGTGGTA
GOX2_F_CDS	qRT-PCR	TTTGCACTAGCTGCTGAAGGA
GOX2_R_CDS	qRT-PCR	ATAACCTGGGCAAATGGCGT
GOX1_F	qRT-PCR	AGAACAGCAGCAACACAGAAC
GOX1_R	qRT-PCR	CACTAGGCTTGGTTTGTGATCTGATA
GOX2_F	qRT-PCR	ATATCTCGAAAAACTTGTTTCTCCCTATAT
GOX2_R	qRT-PCR	ATCTATTGTACAAGCAATAAGAATAAACGG
EF1a_F	qRT-PCR	TCCGTCGGAGCTCAATTCTC
EF1a_R	qRT-PCR	AGGAAGCTCGAGTGCCAAGTAC
UBQ5_F	qRT-PCR	CTGCATTTCTATTTGGGAATTTTGTAA
UBQ5_R	qRT-PCR	ATCCAGAACGAAAGATGTTCAACATAG

Supplemental Table S5. Mutations enriched in line *238.3*.

Chromosome	Position	Reference base	Mutant	Coverage	Frequency	Region	AGI code	Position in gene	Position in codon	Reference amino acid	Mutant
3	4822263	G	A	65	0.9	CDS	*At3g14420*	263	2	G	E
3	7636562	G	A	40	0.89	intergenic					
3	6290758	G	A	60	0.86	intergenic					
3	3807077	G	A	54	0.84	intergenic					
3	6145283	G	A	43	0.83	five_prime_UTR	*At3g17940*				
4	8981113	G	A	5	0.83	intronic/noncoding	*At4g15780*				
3	6021032	G	A	50	0.82	CDS	*At3g17600*	9	3	V	V
3	436295	C	T	60	0.8	CDS	*At3g02260*	11022	3	E	E
3	3397230	G	A	37	0.8	intronic/noncoding	*At3g10845*				
3	6031593	G	A	51	0.8	CDS	*At3g17630*	2223	3	K	K

Supplemental Table S6. Data sources and sequence accessions.

Data source	Species	Accession
PLAZA 3.0 Dicots	*Arabidopsis thaliana*	AT3G14415
		AT3G14420
	Thellungiella parvula	TP3G12710
		TP3G12720
EnsemblPlants release 30	*Arabidopsis lyrata*	fgenesh2_kg.3__1563__AT3G14420.2
	Brassica rapa	Bra021556
		Bra021555
		Bra001550
		Bra001551
		Bra027338
		Bra027339
	Solanum lycopersicum	Solyc07g056540.2
	Solanum tuberosum	PGSC0003DMG400027654
Phytozome 9	*Capsella rubella*	Carubv10014001m.g
		Carubv10013998m.g
	Thellungiella halophila	Thhalv10020979m.g
		Thhalv10020982m.g